YGS • A STUDENT-LED JOURNAL FOR THE SCIENCES AND THE SOCIAL SCIENCES • JUNE 2026

ygs JOURNAL

YOUNG GLOBAL SCIENTISTS

TENTH EDITION

WHO WE ARE

Young Global Scientists (YGS) is an online student-run journal that allows high school students around the world to publish their thoughts, learnings, and discoveries. Our science category includes research papers and science articles, while our social sciences category includes research and opinion pieces on philosophy, politics, history and economics.

YGS was conceived by a group of students at the Yale Young Global Scholars' online summer program. Like YYGS, we provide young voices with a platform to both learn and apply new content by reading and writing YGS articles. All articles are written by students and published in an issue of YGS Journal, available for download on our website. YGS is not only an academic space, it is also a space for connection with youth all around the world. We wish to use our thriving network of young minds to work creatively, receive recognition, and to widen our collective horizons.

WE WANT TO HEAR FROM YOU!

We recognize that for many young scholars around the world, traditional avenues to publication are daunting and often, entirely inaccessible. Our goal is to compile a magazine that showcases some of the most exciting research and opinions from the next generation of thinkers.

GET PUBLISHED:

Please email your work to ygsjournal@gmail.com. In your email, please include your name, the title of your work, and its category–science, social sciences, or the arts.

FIND US AT: HTTPS://WWW.YGSJOURNAL.COM

Contents

UV-Dominated Filamentary Structure in the LINER Galaxy Z97-40: A Multiwavelength Analysis of Rapid Non-Diffusive Gas Redistribution

E. Yenice

April 2026

Abstract

Using optical imaging from the SDSS survey, infrared data, and ultraviolet observations from GALEX, the multiwavelength morphology of the galaxy Z 97-40 is investigated. The object is classified as a LINER-type active galactic nucleus (AGN) in the SIMBAD database.

A significant morphological discrepancy is observed across different wavelength regimes. The structure appears faint and poorly defined in both optical and infrared bands, while in the ultraviolet it exhibits a prominent extended filamentary morphology surrounding the central region.

The absence of a corresponding infrared counterpart suggests a lack of a significant evolved stellar population within the observed structures. In contrast, the ultraviolet emission indicates the presence of recently formed and/or shock-excited gas. The filamentary morphology further indicates that the observed structure is not consistent with a simple diffusive expansion process.

The observed UV-dominated morphology is interpreted as evidence for a rapid, dynamically driven redistribution of gas from the central region, potentially associated with magnetohydrodynamic instabilities or feedback-driven outflow processes.

Several physical mechanisms are considered, including magneto-gravitational instabilities of Parker-type and large-scale feedback-induced transport. However, no single mechanism can be uniquely identified as the dominant driver based on the current dataset.

1 Introduction

The evolution of gas in galactic systems is governed by the coupled effects of hydrodynamics, magnetic fields, and gravitational stratification [Ferrière(2001), Beck(2016)]. Within the framework of magnetohydrodynamics (MHD), ionized

1

interstellar gas behaves as a conducting fluid whose dynamics are described by the continuity, momentum, and induction equations, together with the gravitational potential of the system [Kulsrud(2005), Shu(1992)].

In stratified galactic disks, the interplay between magnetic pressure, gas pressure, and gravity can lead to a variety of instabilities [Boulares & Cox(1990)]. One such mechanism is the Parker instability, which arises when a magnetized medium embedded in a gravitational field becomes unstable to buoyant perturbations [Parker(1966), Parker(1967)]. In this scenario, small deviations from equilibrium can grow, leading to the formation of magnetic loops, filamentary structures, and vertical redistributions of gas. These processes are often discussed in the context of magneto-gravitational instabilities in rotating galactic disks.

The galaxy Z 97-40, classified as a LINER-type active galactic nucleus (AGN) in the SIMBAD database, provides an interesting case for examining the large-scale distribution of ionized gas in a low-luminosity nuclear environment. LINER systems are typically associated with weak nuclear activity, low ionization emission-line regions, and in some cases shock-driven excitation mechanisms rather than strong radiative AGN feedback [Ho(2008)].

Multiwavelength archival data from the Sloan Digital Sky Survey (SDSS), the Galaxy Evolution Explorer (GALEX), and infrared surveys reveal a pronounced discrepancy in the observed morphology of Z 97-40 across different spectral regimes [Martin et al.(2005), Salim et al.(2007)]. The system appears diffuse and weakly structured in optical and infrared bands, while exhibiting a strikingly prominent filamentary morphology in the ultraviolet [Thilker et al.(2007), Boissier et al.(2008)].

This UV-dominated emission suggests the presence of recently formed or shock-excited gas, whereas the lack of a corresponding infrared counterpart implies a deficit of evolved stellar populations within the observed structures [Kennicutt(1998), Leroy et al.(2008)]. The resulting morphology is not readily explained by simple diffusive expansion models, motivating consideration of dynamically driven transport processes.

In particular, magnetohydrodynamic instabilities in stratified rotating disks provide a plausible framework for generating such filamentary and asymmetric structures [Parker(1966), Hanasz & Lesch(2002)]. Among these, Parker-type instabilities, potentially operating in non-axisymmetric modes (e.g., m = 2 symmetry), are considered as a candidate mechanism for producing large-scale bipolar or multi-lobed gas distributions.

However, alternative interpretations, including feedback-driven outflows and tidal perturbations, remain viable. The aim of this study is therefore to characterize the multiwavelength morphology of Z 97-40 and to evaluate the consistency of different physical scenarios with the observed UV-dominated filamentary structure.

2

2 Methods

2.1 Data Acquisition

The analysis of Z 97-40 is based on archival multiwavelength imaging data spanning ultraviolet, optical, and infrared regimes. Ultraviolet observations are obtained from the Galaxy Evolution Explorer (GALEX), optical imaging from the Sloan Digital Sky Survey (SDSS), and infrared data from available archival sky surveys.

All datasets are processed in standard FITS format and reprojected onto a common World Coordinate System (WCS) grid to ensure spatial consistency across wavelength bands [Springel(2005)].

2.2 Image Processing and Calibration

Each dataset is background-subtracted using median sky estimation in source-free regions. Point spread function (PSF) differences between ultraviolet, optical, and infrared data are accounted for by Gaussian smoothing to a common effective resolution [Dobbs et al.(2014)].

Flux calibration is preserved in each band to allow relative surface brightness comparison. The final images are normalized in units of surface brightness for morphological analysis rather than absolute photometry.

2.3 Multiwavelength Morphological Mapping

To quantify structural differences across wavelength regimes, isophotal contour maps are generated for each band. Contours are defined at fixed percentile levels of surface brightness to trace low-intensity extended emission.

A morphological comparison is performed by overlaying UV, optical, and infrared contour maps in a unified coordinate system. Special attention is given to spatial offsets between UV-bright filamentary regions and optically dominant structures.

The UV emission is found to trace extended filamentary features that are not spatially correlated with infrared emission, indicating a decoupling between young stellar populations and evolved stellar components [Thilker et al.(2007)].

2.4 Filament Identification and Geometric Characterization

Filamentary structures in the ultraviolet map are identified using gradient-enhanced edge detection applied to the smoothed surface brightness field. Connected components above a defined signal-to-noise threshold are extracted and treated as coherent structures.

The characteristic angular scale of the dominant filamentary ring structure is measured to be approximately $32''$, corresponding to a projected physical scale dependent on the assumed distance to Z 97-40.

2.5 Conversion to Physical Units

Angular measurements are converted into physical scales using the small-angle approximation:

$$l = D \cdot \theta \tag{1}$$

where D is the distance to the source and θ is the angular size in radians.

This conversion allows estimation of spatial scales relevant to dynamical processes such as rotational shear and magneto-gravitational instabilities [Sellwood(2014)].

2.6 Magnetohydrodynamic Framework

The physical interpretation is based on ideal magnetohydrodynamics (MHD), assuming a single-fluid, fully ionized plasma embedded in a gravitational potential [Kulsrud(2005), Chandrasekhar(1961)]. The governing equations include the continuity equation, momentum conservation, and magnetic induction equation.

The momentum equation is given by:

$$\rho \frac{d\mathbf{v}}{dt} = -\nabla P + \frac{1}{4\pi}(\nabla \times \mathbf{B}) \times \mathbf{B} - \rho \nabla \Phi \tag{2}$$

where P includes both thermal and turbulent contributions.

Magnetic pressure and tension are treated separately, with magnetic pressure defined as:

$$P_B = \frac{B^2}{8\pi} \tag{3}$$

and magnetic tension scaling as:

$$F_T \sim \frac{B^2}{4\pi R_c} \tag{4}$$

where R_c represents the curvature radius of magnetic field lines.

2.7 Instability Analysis Framework

The stability of the system is evaluated by comparing gravitational stratification against magnetic support and gas pressure. In particular, perturbations in a stratified rotating disk are considered under conditions where magnetic tension is insufficient to restore equilibrium.

Under such conditions, buoyancy-driven modes consistent with Parker-type instabilities may develop, leading to vertical displacement of magnetized gas and the formation of filamentary structures [Parker(1966)].

Non-axisymmetric perturbations are considered, including modes with azimuthal symmetry $m = 2$, which can produce bipolar or double-lobed morphological features depending on the background magnetic field geometry and rotation profile[Jog(1992), Romeo & Falstad(2013)].

2.8 Interpretation Strategy

Rather than attributing a unique physical mechanism, the methodology follows a comparative framework in which multiple scenarios (magneto-gravitational instability, feedback-driven outflows, and tidal perturbations) are evaluated against the observed multiwavelength morphology. The goal is to identify which physical processes are most consistent with the observed UV-dominated filamentary structure.

3 Results

3.1 Multiwavelength Morphology

The multiwavelength comparison of Z 97-40 reveals a strong morphological discrepancy between ultraviolet, optical, and infrared regimes.

The ultraviolet (GALEX) image shows a dominant extended filamentary structure surrounding the central region, while the optical and infrared data exhibit significantly weaker emission, with morphology concentrated toward the inner region and lacking extended structural features [Thilker et al.(2007), Boissier et al.(2008)].

3.2 UV-Dominated Structure and Dynamical Implications

From a magnetohydrodynamic perspective, such a strong wavelength-dependent decoupling suggests that the emitting plasma is not in a simple thermodynamic equilibrium state [Kulsrud(2005)]. Instead, the morphology is consistent with a magnetized, stratified medium in which magnetic forces play a significant role in structuring the gas distribution [Ferrière(2001), Beck(2016)].

The ultraviolet emission appears to define a coherent large-scale filamentary structure that is not traced by the older stellar population indicators in the infrared band.

To further quantify the spatial distribution of the emission, isophotal contour maps are constructed for each wavelength regime.

The comparison between contour maps across different wavelengths demonstrates a clear decoupling between ultraviolet and infrared emission structures.

In a diffusive regime, both magnetic fields and gas distributions would evolve toward smoother and more correlated large-scale structures [Kulsrud(2005)]. However, the presence of sharp, coherent filamentary features in the ultraviolet band, without corresponding optical or infrared counterparts, is inconsistent with a purely diffusive evolution [Thilker et al.(2007)]. This suggests that the observed morphology is governed by dynamically driven processes rather than resistive smoothing.

Within the framework of magnetohydrodynamics, such filamentary structures can arise in a stratified galactic disk where the competition between gravitational force, gas pressure, and magnetic tension leads to buoyancy-driven instabilities [Parker(1966)]. In particular, when magnetic tension is insufficient

5

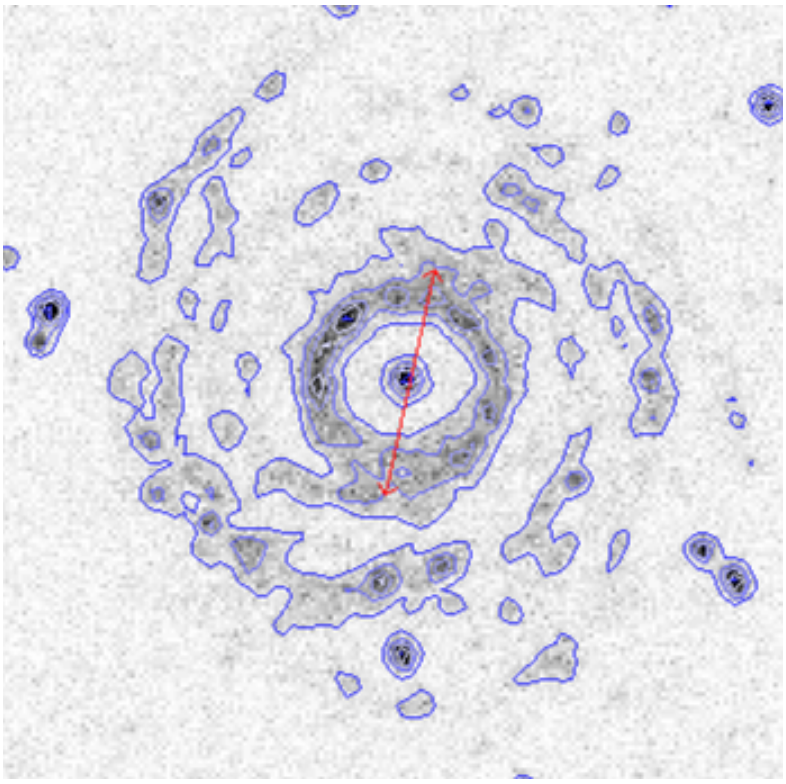

Figure 1: Far-ultraviolet (FUV) image of Z 97-40 obtained from GALEX. The emission is dominated by an extended filamentary structure surrounding the central region. A red bidirectional arrow is overplotted, passing through the galactic center and connecting the two dominant UV-bright lobes. This annotation highlights an approximate 180° angular separation and indicates the location of a possible $m = 2$ symmetry candidate in the large-scale gas distribution.

to counteract vertical displacement of magnetized gas, Parker-type modes may develop, producing loop-like and filamentary structures aligned with the magnetic field geometry [Parker(1967)].

3.3 Outflow Geometry and Symmetry

A prominent morphological feature of the ultraviolet structure is its apparent bipolar or double-lobed geometry, with a projected angular scale of approximately $32''$. This configuration suggests a possible $m = 2$ symmetry mode in the large-scale gas distribution, potentially arising from non-axisymmetric perturbations in a rotating magnetized medium [Jog(1992), Romeo & Falstad(2013)].

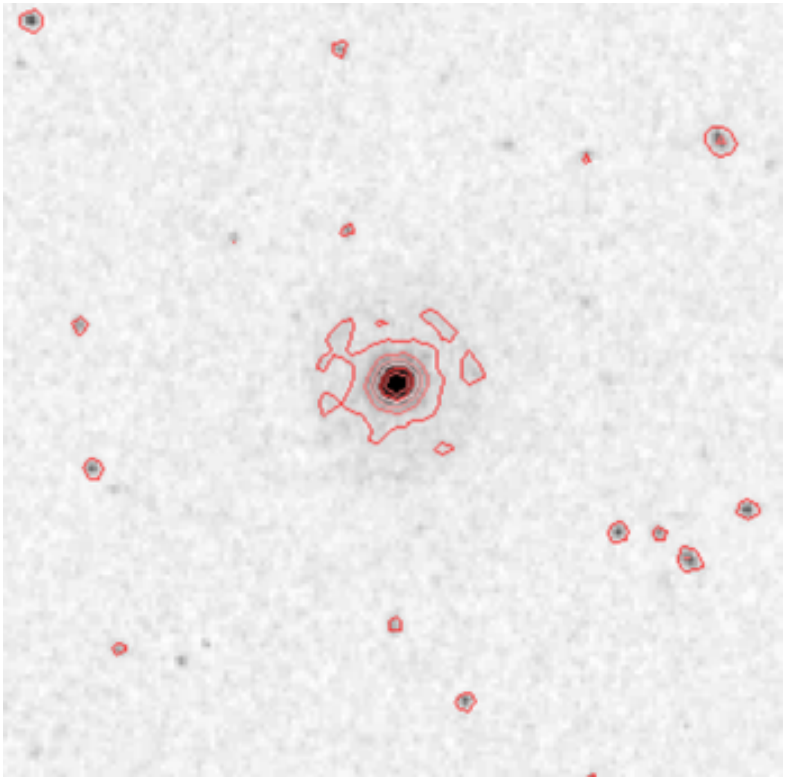

Figure 2: Optical (SDSS) image of Z 97-40. The structure appears diffuse with weak large-scale features, indicating a lack of strong stellar population correlation with the ultraviolet filamentary morphology.

3.4 Physical Interpretation

The combined multiwavelength evidence indicates a rapidly evolving gas structure dominated by ultraviolet-bright filamentary features, with minimal contribution from older stellar populations.

4 Discussion

4.1 Possible Physical Origins of the UV Morphology

The origin of the extended ultraviolet filamentary structure in Z 97-40 can be interpreted under several competing physical scenarios. Given the absence of direct kinematic measurements, the following discussion is based on morphological and multiwavelength constraints only.

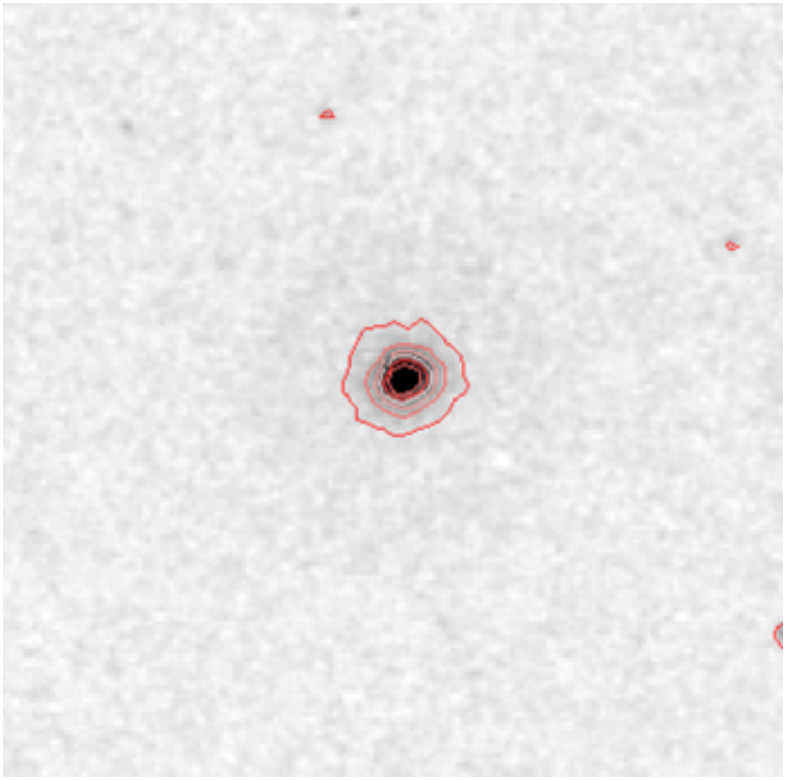

Figure 3: Infrared image of Z 97-40. The emission is centrally concentrated with minimal extended structure, suggesting a deficit of evolved stellar populations in the regions traced by UV emission.

4.2 Feedback-Driven Outflows

AGN or stellar feedback processes can generate large-scale outflows and filamentary structures through mechanical energy injection and radiative pressure [Veilleux et al.(2005)]. However, Z 97-40 is classified as a LINER-type nucleus, indicating relatively weak nuclear activity [Ho(2008)]. In addition, the infrared emission does not show evidence of strong centrally concentrated starburst activity.

These constraints make a strong feedback-driven outflow scenario less favorable as the primary mechanism, although localized feedback effects cannot be fully excluded.

4.3 Tidal Interaction Scenario

Tidal interactions with a companion galaxy can produce asymmetric, filamentary, and extended morphological features [Kormendy & Ho(2013)]. Such pro-

8

cesses typically also leave signatures in the stellar distribution traced by optical and infrared bands.

In the case of Z 97-40, the ultraviolet emission is strongly decoupled from both optical and infrared morphologies, with no clear corresponding stellar tidal features. While a past interaction cannot be ruled out, the lack of multiwavelength structural coherence weakens a purely tidal origin interpretation.

4.4 Magneto-Gravitational Instability (Parker-Type Scenario)

Within a magnetized, stratified galactic disk, buoyancy-driven instabilities can naturally arise when magnetic tension is insufficient to stabilize vertical perturbations in the gas layer [Parker(1966)]. Such Parker-type modes can produce loop-like and filamentary structures aligned with the magnetic field geometry, particularly in environments with strong vertical stratification [Hanasz & Lesch(2002)].

The observed ultraviolet morphology of Z 97-40, characterized by coherent filamentary structures and a pronounced decoupling from infrared emission, is qualitatively consistent with such magneto-gravitational instability-driven evolution [Koyama & Ostriker(2009), Ostriker et al.(2010)].

In this context, the apparent large-scale symmetry of the UV structure may reflect a non-axisymmetric response of the disk to magnetic and gravitational forces.

4.5 Scenario Ranking

Based on the current observational constraints, the following qualitative ranking of scenarios is proposed:

1. **Magneto-gravitational (Parker-type) instability:** Most consistent with UV filamentary morphology and wavelength decoupling.
2. **Tidal interaction:** Possible but lacks supporting multiwavelength stellar signatures.
3. **Feedback-driven outflows:** Least favored due to weak nuclear activity indicators.

4.6 Limitations

This study is limited by the absence of kinematic data, including velocity fields and gas-phase diagnostics. As a result, the proposed interpretations remain morphological and cannot be uniquely distinguished. Future spectroscopic observations would be required to confirm the presence of ordered outflows, rotation signatures, or magnetic field constraints.

9

5 Conclusion

We present a multiwavelength morphological analysis of the LINER-type galaxy Z 97-40 using ultraviolet (GALEX), optical (SDSS), and infrared archival data. The system exhibits a pronounced discrepancy between UV emission and longer wavelength tracers, with the ultraviolet band revealing a coherent filamentary structure that is not mirrored in optical or infrared maps.

Isophotal contour analysis confirms a strong spatial decoupling between ultraviolet and infrared emission, suggesting that the observed morphology is not governed by a single, smoothly evolving stellar population. Instead, the structure appears to be dominated by dynamically reorganized gas.

The UV morphology shows an approximate bipolar geometry with a projected angular scale of $\sim 32''$, indicating a possible $m = 2$ symmetry in the large-scale emission distribution. However, in the absence of kinematic constraints, this interpretation remains morphological.

We explored several physical scenarios for the origin of the observed structure. Feedback-driven outflows and tidal interactions are found to be less favored due to the lack of corresponding multiwavelength signatures. In contrast, magneto-gravitational instability scenarios, particularly Parker-type modes in a stratified magnetized disk, provide a qualitatively consistent framework for the observed filamentary UV structure and wavelength-dependent decoupling.

We emphasize that the present study is purely morphological and does not constitute a direct detection of any instability mode. Future spectroscopic and kinematic observations will be essential to distinguish between competing physical mechanisms and to test the proposed interpretation.

References

[Parker(1966)] Parker, E. N. 1966, ApJ, 145, 811
https://doi.org/10.1086/148828

[Parker(1967)] Parker, E. N. 1967, ApJ, 149, 535
https://doi.org/10.1086/149282

[Kulsrud(2005)] Kulsrud, R. M. 2005, Plasma Physics for Astrophysics
https://doi.org/10.1515/9780691213354

[Ferrière(2001)] Ferrière, K. M. 2001, Rev. Mod. Phys., 73, 1031
https://doi.org/10.1103/RevModPhys.73.1031

[Beck(2016)] Beck, R. 2016, A&ARv, 24, 4
https://doi.org/10.1007/s00159-015-0084-4

[Boulares & Cox(1990)] Boulares, A., & Cox, D. P. 1990, ApJ, 365, 544
https://doi.org/10.1086/169509

[Kennicutt(1998)] Kennicutt, R. C. 1998, ARA&A, 36, 189
https://doi.org/10.1146/annurev.astro.36.1.189

[Martin et al.(2005)] Martin, D. C., et al. 2005, ApJ, 619, L1
https://doi.org/10.1086/426387

[Salim et al.(2007)] Salim, S., et al. 2007, ApJS, 173, 267
https://doi.org/10.1086/519218

[Thilker et al.(2007)] Thilker, D. A., et al. 2007, ApJS, 173, 538
https://doi.org/10.1086/523853

[Boissier et al.(2008)] Boissier, S., et al. 2008, ApJ, 681, 244
https://doi.org/10.1086/588580

[Leroy et al.(2008)] Leroy, A. K., et al. 2008, AJ, 136, 2782
https://doi.org/10.1088/0004-6256/136/6/2782

[Veilleux et al.(2005)] Veilleux, S., et al. 2005, ARA&A, 43, 769
https://doi.org/10.1146/annurev.astro.43.072103.150610

[Hanasz & Lesch(2002)] Hanasz, M., Lesch, H. 281, 289–292 (2002).
https://doi.org/10.1023/A:1019576612600

[Hanasz et al.(2004)] Hanasz, M., et al. 2004, ApJ, 605, L33
https://doi.org/10.1086/420936

[Koyama & Ostriker(2009)] Koyama, H., & Ostriker, E. C. 2009, ApJ, 693, 1316
https://doi.org/10.1088/0004-637X/693/2/1316

[Ostriker et al.(2010)] Ostriker, E. C., et al. 2010, ApJ, 721, 975
https://doi.org/10.1088/0004-637X/721/2/975

[Sellwood(2014)] Sellwood, J. A. 2014, Rev. Mod. Phys., 86, 1
https://doi.org/10.1103/RevModPhys.86.1

[Dobbs et al.(2014)] Dobbs, C. L., et al. 2014, Protostars and Planets VI
https://doi.org/10.1017/pasa.2014.31

[Shu(1992)] Shu, F. H. 1992, The Physics of Astrophysics

[Spitzer(1978)] Spitzer, L. 1978, Physical Processes in the Interstellar Medium
https://doi.org/10.1002/9783527617722

[Chandrasekhar(1961)] Chandrasekhar, S. 1961, Hydrodynamic and Hydromagnetic Stability

[Jog(1992)] Jog, C. J. 1992, ApJ, 390, 378
https://doi.org/10.1086/171289

[Romeo & Falstad(2013)] Romeo, A. B., & Falstad, N. 2013, MNRAS, 433, 1389
https://doi.org/10.1093/mnras/stt809

[Springel(2005)] Springel, V. 2005, MNRAS, 364, 1105
https://doi.org/10.1111/j.1365-2966.2005.09655.x

[Ho(2008)] Ho, L. C. 2008, ARA&A, 46, 475
https://doi.org/10.1146/annurev.astro.45.051806.110546

[Kormendy & Ho(2013)] Kormendy, J., & Ho, L. C. 2013, ARA&A, 51, 511
https://doi.org/10.1146/annurev-astro-082708-101811

Quantifying Color Use in European Painting, 1230–1950: A Computational Analysis of Long-Term Artistic Change

Gan Chen

1. Abstract

Color has been the focus of European painting research for a long time, and it not only played a role in visual composition, but also carried cultural connotations (Gage, 1993). Art historians generally believe that the change of color is inevitably related to changes in aesthetic preferences, art techniques, and patronage (Ball, 2001). In the development of medieval painting, the color is relatively monotonous, but with the development of industrial technology, the color is more and more abundant, which is inevitably related to the historical context (Ball, 2001).

In the process of writing art history, attention should be paid to analyzing the role of color in the development of a specific period and movement. In the Renaissance period, the color of the painter's work is balanced and harmonious, which is consistent with the naturalism theory (Baxandall, 1988). In Baroque art, the contrast is more intense, and the emotional expression is stronger (Encyclopaedia Britannica, 2026). In the modern period, some theorists believe that color can express the inner state of people, not just describe (Kandinsky, 1911). However, these interpretations are typically derived from close visual analysis of individual works and do not establish whether such patterns hold consistently across large datasets.

1. 1 Literature Review

In recent years, the rapid development of digital technology and the continuous upgrading of image analysis technology have changed the traditional research mode, and the construction of visual culture has achieved breakthrough progress. With the support of high-resolution images and the promotion of metadata, the traditional research mode can not meet the needs of the development of the times, and the open access initiative launched by the Metropolitan Museum of Art can provide more public domain images for the public, which can support large-scale comparative analysis (The Metropolitan Museum of Art, 2017).

With the rapid development of data science and computer vision, it is possible to extract visual features from images in a systematic and repeatable way, and the extracted visual features are quantifiable, including brightness, saturation and other contents. In the field of computational art history, scholars have constructed large data sets to analyze whether the visual features obtained through measurement or learning are consistent with the historical categories, and to find that quantitative analysis can reveal the structure corresponding to art history (Elgammal et al. , 2018). Digital art history also points out that the updating of digital standards and the rapid development of computer vision have brought changes to scholars in the study of large image corpora, and scholars are still debating the responsibility of interpretation and the development of disciplines (Brey, 2021).

In the development of digital art history, scholars have repeatedly pointed out that the quality of digital reproduction is relatively low, and there are obvious differences between different images (Zorich, 2012). In the process of digitization, the color management, lighting and so on are different, which will have an impact on the measurement of color characteristics. Therefore, it is necessary to have a sound digital standard system, which requires the use of unified workflow and reasonable color management (FADGI, 2023). The above problems are the focus of attention in the study of museum images (FADGI, 2023).

1. 2 Gap

Although there are breakthroughs in methodology, the interpretation of color in the development of art history is still relatively qualitative, and it is difficult to systematically analyze the changes in a long historical period. Most of the computational work in the process of analyzing the paintings focuses on classification and prediction, but does not analyze the changes of multiple colors from the time dimension (Elgammal et al. , 2018). The development of digital art history has gradually improved the standards, tools and interpretation framework, and how to coordinate the relationship between computational description and humanistic explanation has become a key issue (Brey, 2021).

In order to make up for this deficiency, this project aims to use large-scale calculation methods to analyze the development of European painting from 1230 to 1950, and to grasp the evolution of color in this period. In this study, 1700 public domain works were selected from the Metropolitan Museum of Art to analyze the color from four dimensions: saturation, brightness,

hue distribution and style color deployment. Through the analysis of the above four aspects, the long-term development trend is grasped, and the color practice of painters in the past eight centuries is described with the help of data. This method can not only analyze the color from the macro level, but also analyze the visual level, which can better explain the narrative of artistic change.

2. Method and Process

2. 1 Data Construction and Processing

In this study, the data set is constructed, which includes metadata and image data, and the color evolution of European paintings is analyzed in depth. The data set includes 1781 European paintings, with a time span of more than 700 years, and the data comes from the Open Access collection of the Metropolitan Museum of Art. Each painting has a unique digital image and metadata, including the name of the work, the name of the author, the production date, etc.

In order to make the analysis more reasonable, the average production year is calculated as the midpoint between the start date and the end date, and the paintings are divided into several groups according to the decade variable. In this way, the noise of a single work can be reduced, and the style trajectory of the seven centuries can be analyzed.

All color indicators can be extracted from image data. Open source Python library can be used in this process, which can load images (Clark, 2015), process numerical data (Harris et al. , 2020), and transform color space (van der Walt et al. , 2014).

In order to ensure the comparability of the obtained images and to unify the resolution and size, all color variables should be standardized, and the pixel share and average value should be unified. This is a normal practice to ensure that the measurement results are related to the absolute pixel count and the relative color structure. In the process of digital reproduction, there are many influencing factors, and the measurement results are inevitably affected by artistic decisions and digital technology. In the process of sample aggregation, the influence of image variation is relatively small, and the historical pattern can be obtained.

See **Table A1** in **Appendix A** for a complete list of variables, definitions and descriptive statistics.

2. 2 Feature Extraction Methods

In order to make the color have a multi-dimensional connotation, the image features are divided into four parts: luminance, saturation, hue and style.

2. 2. 1 Luminance-based metrics

In order to grasp the brightness and tone structure, the RGB image is converted into relative luminance by using the standard perception luminance equation (Fairchild, 2013):

$$L = 0.2126R + 0.7152G + 0.0722B \quad (1)$$

In this study, the normalized channel value is taken as the research object, and the luminance map is constructed to calculate the statistical indicators, including mean luminance, standard deviation, 10th percentile luminance and 90th percentile luminance, which can describe the shadow area and highlight area respectively, and also calculate the proportion of dark pixels below a certain luminance threshold. In the process of calculation, the overall brightness, the contrast between the two tones, and the proportion of light and dark areas in the picture are taken as the main indicators.

2. 2. 2 Chroma and Saturation Measures

The color saturation and chroma of the product were evaluated. Harris et al. (2020) used the channel range method to calculate the chroma.

$$C = max(R, G, B) - min(R, G, B) \quad (2)$$

The chromaticity is calculated to measure the color contrast. The threshold method is used to calculate the proportion of pixels with high and low chroma. At the same time, the images are converted into HSV color space, and the color purity is measured by saturation (Smith, 1978):

$$S = \frac{C}{V},\ where\ C = V - min(R, G, B)\ and\ V = max(R, G, B) \quad (3)$$

Mean saturation was retained as a complementary indicator of overall color intensity.

2. 2. 3 Hue Distribution Analysis

HSV space can divide hue into 12 categories, which can be divided into equal angular bins. The proportion of pixels in each category is calculated for each work, and the normalized hue variable is obtained (such as blue, orange, red, etc.). This method can reduce the complexity

of pixels, make up for the shortcomings of the previous method, and can compare the differences between different colors (Itten, 1970).

2. 2. 4 Stylistic Color Deployment Metrics

In addition to color, style deployment also needs to pay attention to how to organize colors in the whole composition. When classifying pixels, the saturation and brightness are used as the standard, which can be divided into several categories: "low saturation and high brightness", "low chroma", "high saturation" and so on. The brightness and saturation are global indicators. The use of these indicators can describe art history, and can make a quantitative description of "neutral", "pastel" and other terms.

2. 3 Statistical Analysis

2. 3. 1 Temporal Trend Analysis

Each decade is a statistical unit, and all color indicators are aggregated. Trend charts are used to grasp the changes of brightness, intensity and hue in the direction of time from the 13th to the 20th century.

2. 3. 2 Correlation and Distributional Analysis

In order to analyze the relationship between the color dimension and the painting, the Pearson coefficient is introduced for analysis (Pearson, 1895):

$$r = \frac{\Sigma(x_i-\underline{x})(y_i-\underline{y})}{\sqrt{\Sigma(x_i-\underline{x})^2\,\Sigma(y_i-\underline{y})^2}} \qquad (4)$$

The analysis focuses on theoretically relevant variable pairs, including brightness and color intensity, saturation and chroma, as well as tonal structure and hue distribution. These relationships help identify how different visual properties interact within paintings rather than functioning independently. By examining these associations across a large dataset, the study captures consistent structural patterns in color usage.

This method does not analyze a single work, but describes the development pattern of a large number of samples. By integrating the advantages of the above methods, the study systematically describes the changes in color in the process of European painting development.

3. Results

3. 1 Data Processing Result

After the Met Open Access collection is filtered, the image can be used for a period of time, and the data set finally includes 1781 works. For each painting, the color characteristics of pixels are extracted, and the luminance, saturation, hue and other indicators are summarized. All the data are calculated from the normalized pixel values, which can guarantee the consistency of the resolution of each image. The data are aggregated by decade to support the analysis of long-term trends and to eliminate the impact of noise caused by a single work.

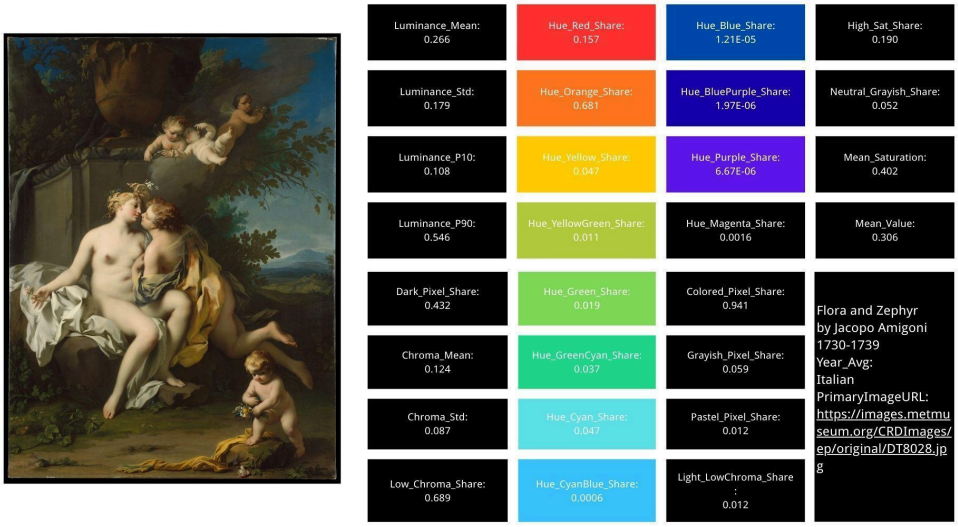

Figure 1: Color metrics output (Jacopo Amigoni, Flora and Zephyr, 1730-1739, The Metropolitan Museum of Art, 2025)

3. 2 Color Usage Trends Across Decades

The color usage of European paintings is analyzed from the long-term perspective, and the color metrics are analyzed in depth at the level of ten years. Drawing on hue, brightness and other indicators, the changes of color intensity, color family and so on in the period of 1230-1950 are analyzed. Through the analysis of the time trend line, the color practice of painters in the process of a thousand years is analyzed, and the empirical baseline is provided for the interpretation of style transformation, transition and so on. In the text, the most prominent inflection points and long-term development are analyzed, and the statistical summaries of each chart are listed in Table 2 for reference. In **Appendix B**, there are a series of visualizations

corresponding to the results, including all the trend line charts in **Section 3. 2. Appendix B and Table 2** are the basis for the interpretation of the trend analysis.

A note on sampling

The number of works in the Met dataset is relatively small, and the number of decades is relatively small. If a series of metrics show sharp changes at the same time, it is likely that the sample size is too small, but there is no sudden change in style.

Table 2: Color change trend of European paintings (1230-1950)

Variable	Graph Serial	Slope	Net Δ	Peak (value @decade)	Trough (value @decade)	Med	EarlyMod	Modern
Luminance_ Mean	B1	-6. 50E-05	0. 189	0. 448 @1360	0. 195 @1690	0. 351	0. 246	0. 328
Dark_ Pixel_ Share	B2	1. 25E-04	-0. 476	0. 638 @1650	0. 0123 @1950	0. 309	0. 524	0. 352
Luminance_ Std	B3	-9. 94E-05	-0. 092	0. 323 @1360	0. 078 @1950	0. 209	0. 154	0. 167
Luminance_ P10	B4	9. 08E-05	0. 332	0. 331 @1950	0 @1230	0. 085	0. 077	0. 131
Luminance_ P90	B4	-2. 21E-04	0. 048	0. 914 @1360	0. 346 @1690	0. 642	0. 460	0. 552
Chroma_ Mean	B5	-1. 42E-04	-0. 073	0. 332 @1340	0 @1360	0. 186	0. 109	0. 119
Chroma_ Std	B6	-9. 91E-05	-0. 101	0. 190 @1390	0 @1360	0. 125	0. 080	0. 080
Low_ Chroma_ Share	B7	4. 08E-04	0. 268	1 @1360	0. 206 @1340	0. 506	0. 729	0. 690
High_ Chroma_ Share	B7	-2. 69E-04	-0. 075	0. 421 @1340	0 @1360	0. 149	0. 016	0. 025
Hue_ Red_ Share	B8	-1. 26E-04	-0. 284	0. 514 @1470	0 @1360	0. 333	0. 338	0. 259
Hue_ Orange_ Share	B8	1. 72E-04	0. 371	0. 806 @1950	0 @1360	0. 393	0. 447	0. 456

Hue_ Yellow_ Share	B8	9. 80E-05	0. 043	0. 105 @1740	0 @1360	0. 017	0. 059	0. 063
Hue_ YellowGreen_ Share	B8	2. 58E-05	0. 014	0. 048 @1890	0 @1360	0. 006	0. 013	0. 019
Hue_ Green_ Share	B8	2. 04E-05	0. 014	0. 048 @1910	0@1360	0. 006	0. 010	0. 017
Hue_ GreenCyan_ Share	B8	3. 13E-05	0. 030	0. 120 @1910	0@1360	0. 011	0. 018	0. 026
Hue_ Cyan_ Share	B8	-4. 28E-06	-0. 128	0. 163 @1230	0 @1360	0. 036	0. 033	0. 038
Hue_ CyanBlue_ Share	B8	-7. 91E-06	-0. 047	0. 068 @1410	0 @1360	0. 015	0. 007	0. 013
Hue_ Blue_ Share	B8	1. 35E-06	-0. 003	0. 028 @1420	0 @1360	0. 003	0. 002	0. 004
Hue_ BluePurple_ Share	B8	3. 99E-06	-0. 001	0. 030 @1910	0 @1360	0. 001	0. 001	0. 003
Hue_ Purple_ Share	B8	5. 78E-06	-0. 001	0. 037 @1910	0 @1360	0. 001	0. 001	0. 005
Hue_ Magenta_ Share	B8	-1. 53E-06	-0. 009	0. 03425 @1570	0 @1360	0. 009	0. 010	0. 009
High_ Sat_ Share	B9	-3. 42E-04	-0. 460	0. 5933 @1370	0 @1360	0. 363	0. 255	0. 200
Neutral_ Grayish_ Share	B9	-2. 01E-04	-0. 049	1 @1360	0. 051 @1730	0. 278	0. 166	0. 213
Pastel_ Pixel_ Share	B10	-1. 31E-05	4. 91 E-04	0. 3086 @1360	3. 31E-04 @1230	0. 066	0. 029	0. 066

Light_ LowChroma_ Share	B10	-1. 45E-05	0. 004	0. 3468 @1360	4. 52E-04 @1230	0. 072	0. 033	0. 071
Mean_ Saturation	B11	-1. 00E-04	-0. 210	0. 5552 @1340	0 @1360	0. 393	0. 381	0. 334

Table 2 summarizes the main conclusions of the analysis of the development trend over the past ten years, and introduces the structural characteristics of European painting in the period from the 1230s to the 1950s. Luminance measurement can grasp the nonlinear trajectory, with high brightness and strong color variability in the fourteenth century, but in the early modern period, the color gradually darkened, the proportion of dark pixels increased, and the color contrast weakened. From the eighteenth century, the brightness gradually increased, and the highlight was more prominent, but the shadow was not eliminated. This is a reasonable balance between light and dark.

Chroma is an important indicator. The transition from the Middle Ages to the early modern period is a parallel shift. After the 15th century, the chroma is relatively low, and the chroma is weak for several centuries, but it has recovered slightly in the 19th century. The chroma of the early modern period is relatively low, which means that the color intensity is redistributed in the structural level, not that the color intensity disappears. Hue distribution has a strong stability, although the proportion of cold colors has increased slightly, orange and red have always been the dominant colors, and the proportion of neutral gray regions has remained unchanged in the long-term development, while the saturation has declined and the pastel strategy has been adopted. In general, the development of European painting has not undergone a sudden change, but the color intensity and brightness have changed in the stable chromatic framework.

In order to make it more intuitive, this paper draws a histogram to describe the change of hue distribution in the last ten years, and divides it into twelve categories (see Appendix B for the trend line).

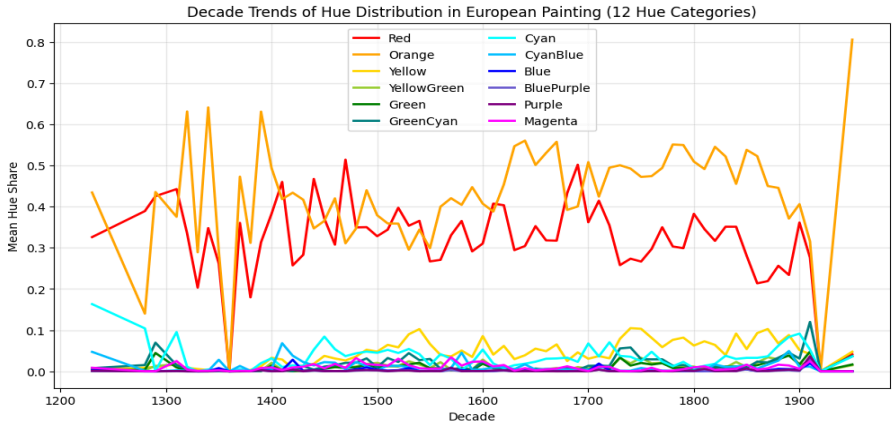

Figure 2: Decade Trends of Hue Distribution in European Painting (12 Hue Categories)

Figure 2 shows that the chromatic hierarchy of European paintings has remained stable for a long time. Warm colors occupy a large area in the painting, and the color structure is relatively stable. Orange is the most common color in modern paintings, while red is the most common color in the early period, and the proportion of red gradually decreases with the passage of time. In the 1700s, the proportion of yellow and green increased, which was related to the increase of landscape paintings, but the proportion was not high. Blue, purple and other colors are relatively low, and the use of cool colors is relatively small, which can only play an auxiliary role. Although there are some fluctuations in the decade, the color structure of the whole painting has not changed significantly, and the color of the painting has always been relatively warm, and the change of secondary color has not changed the color structure.

3. 3 Correlation Analysis

Trend line analysis captures how color variables change over time, allowing for the identification of long-term patterns rather than isolated variation. By examining shifts in luminance, chroma, saturation, and hue distribution across decades, the analysis reveals gradual changes in visual strategies. In addition, correlation analysis evaluates how these variables interact, providing insight into whether changes in one dimension are associated with changes in another. Together, these methods offer a complementary understanding of both temporal development and structural relationships in color usage.

Table 3. Summary of Pearson Correlation Analyses Among Color Metrics (Painting-Level Data)

Figure	X (predictor)	Y (outcome)	Pearson r	p-value	n	OLS	Intercept

						slope (y~x)	
Figure C1	Luminance_Mean	Mean_Saturation	-0. 3851	4. 82E-64	1781	-0. 4740	0. 5123
Figure C2	Luminance_Mean	Chroma_Mean	0. 2560	4. 85E-28	1781	0. 1354	0. 0851
Figure C3	Dark_Pixel_Share	Mean_Saturation	0. 2770	9. 63E-33	1781	0. 1677	0. 3023
Figure C4	Mean_Saturation	Chroma_Mean	0. 6727	5. 36E-235	1781	0. 2890	0. 0138
Figure C5	High_Sat_Share	High_Chroma_Share	0. 4752	5. 10E-101	1781	0. 1684	-0. 0105
Figure C6	Hue_Blue_Share	Luminance_Mean	0. 0583	0. 0139	1779	0. 5737	0. 2799
Figure C7	Hue_Yellow_Share	Mean_Value	0. 0060	0. 7988	1779	0. 0088	0. 3301
Figure C8	Hue_Orange_Share	Mean_Saturation	0. 2940	8. 33E-37	1779	0. 1900	0. 2917
Figure C9	High_Sat_Share	Neutral_Grayish_Share	-0. 4237	1. 69E-78	1781	-0. 4497	0. 2827
Figure C10	Pastel_Pixel_Share	Mean_Saturation	-0. 4620	6. 94E-95	1781	-0. 7056	0. 4098
Figure C11	Low_Chroma_Share	High_Chroma_Share	-0. 5916	1. 33E-168	1781	-0. 2076	0. 1756

Through the analysis of **Table 3** as shown above, it is known that the three dimensions are closely related to each other, and there is a significant relationship between them. From the analysis, the color intensity and brightness of the painting are not strictly unified, and the saturation and brightness are negatively related ($r = -0.385$, $p < 0.001$). It can be seen that the brightness of the painting is relatively high, and the saturation of the color is relatively low. However, there is a positive relationship between luminance and chroma ($r = 0.256$, $p < 0.001$), which means that even if the saturation is low, the work with high brightness can still have a strong contrast between the structure and the channel. It can be seen that the brightness and saturation are positively related ($r = 0.277$, $p < 0.001$), which means that the composition with low brightness can be more saturated. The above conclusions show that brightness, saturation and chroma are interrelated, but they are different in color practice.

In the process of internal consistency test, the color metric can be analyzed in depth, and its logicality is relatively strong. There is a strong positive relationship between average saturation and average chromaticness (r=0. 673, p<. 001), which proves that the two indicators are related to intensity. Threshold measurement is consistent, the higher the saturation, the higher the chroma (r=0. 475, p<. 001). At the same time, the strong negative relationship is also reflected in the style opposition. There is an inverse relationship between high saturation and gray share (r=-0. 424, p<. 001), and there is also a negative relationship between pastel share and average saturation (r=-0. 462, p<. 001). The relationship between low chroma share and high chroma share is also negative (r=-0. 592, p<. 001). The above inverse relationship is consistent, which shows that the deployment metric can capture the exclusive style strategy.

In the process of describing the relationship between color and tone, greater caution should be exercised. The proportion of blue is positively related to brightness, but the correlation coefficient is only 0. 058, and the significance level is 0. 014, which is not significant. The proportion of yellow is not significantly related to brightness, with a correlation coefficient of 0. 006 and a significance level of 0. 799, which means that these two colors can not predict the tone. There is a moderate positive relationship between the proportion of orange and saturation, with a correlation coefficient of 0. 294 and a significance level of less than 0. 001, which means that orange can be used as a marker to describe chromaticity, but not brightness. From the whole point of view, the correlation matrix can show the relationship between hue, saturation, brightness and chroma, and can also reflect the relationship between structured and interpretable, especially the relationship between tone darkness and saturation, which is consistent with the data set. The analysis is based on the data of painting level, which only describes the relationship between the two variables, not the causal relationship.

In order to explain the relationship between the two, the relationship between mean saturation and mean chroma is taken as an example, and the relationship between the two is consistent. In the appendix, the author draws a series of charts to describe the relationship between the two.

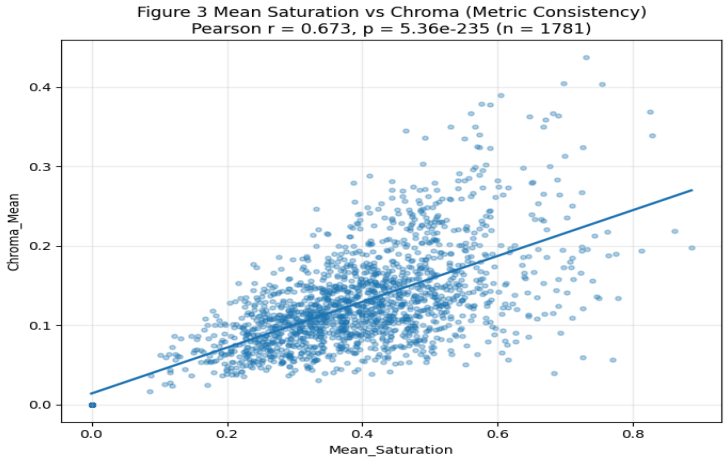

Figure 3 Mean Saturation vs Chroma (Metric Consistency)

Figure 3 shows the relationship between chroma and saturation in all the works in the data set. After analysis, it is found that the two indicators have a strong positive correlation (r = 0. 673, p <. 001, n = 1781), which means that the higher the saturation, the greater the chromatic variation. The regression line is increasing, and the clustering is relatively tight, which is significantly different from other correlation tests. This conclusion further shows that the two indicators are consistent in all works, and the changes are relatively stable.

However, it should be noted that the relationship between the two is not perfect, which is enough to show that the two are related but there are differences. Saturation describes the purity of the color, which is a concept in HSV space, and chroma is the spread of the numerical channel in RGB space. The strong relationship between the two shows that the measurement framework has good internal consistency, and the two indicators do not have perfect consistency, which shows that they can grasp the color intensity in different ways, and the two indicators are not redundant, but complementary, so the two indicators can be retained in the analytical model, which is enough to show that the color behavior in European painting has a certain structure and is meaningful.

4. Discussion

As mentioned before, the research focuses on how to make up for the shortcomings of the previous method, and analyze the relationship between the color practice and the change of style in the narrative of art history. Qualitative analysis shows that the use of this method can describe

the evolution of color in a more reasonable way, and can also analyze the changes of hue, saturation and other contents in the development of European painting.

4. 1 Interpretation of Long-Term Color Trajectories

The results indicate that the color of European paintings has changed in the process of development, and the changes of chromaticity and tone are relatively gentle, not too abrupt. The analysis of luminance pattern shows that the brightness of early works is relatively low, and the brightness of works in the early modern period is relatively low, but the brightness has been balanced in the later period, which shows that the changes of light and shadow in the process of development are relatively balanced, not directional.

From the trend of chroma and saturation, it can be seen that the color intensity has been relatively weak for a long time, and there has been a slight recovery in the later period. The expansion of low chroma areas shows that even if the colors are relatively strong in some periods, the tonal foundation is relatively weak. Generally speaking, the evolution of style is related to the adjustment of emphasis, and the visual system will not change.

4. 2 Structural Relationships Among Color Dimensions

Through correlation analysis, it is known that the use of color in different dimensions can interact with each other in a reasonable way. The negative relationship between saturation and brightness indicates that the two are competitive in the process of visual analysis, and the positive relationship between saturation and chroma shows that the two are consistent.

There is a strong negative correlation between different styles, which is enough to show that artists are willing to use dominant strategies in the process of composition, and do not pursue extremes. Therefore, it can be seen that the change of style is not accidental, but the result of the balance between many visual properties, and the color is no longer an isolated feature, but a variable that is interdependent.

4. 3 Methodological Implications

The above research results show that the research methods of art history have been extended to computational analysis. In the study, the qualitative concept is transformed into a measurable variable, which can analyze the data comprehensively and compare the data for a

long time. This is different from the traditional analysis method, which focuses on the analysis of a single work, and can accurately grasp the macro pattern.

The findings further proves that the interpretation should be carried out carefully. In the analysis, digital images are used as tools, and color values are measured, which can reflect the artistic decisions and reproduction content of the works. Although the research results are similar, it is necessary to use the computational method to build a reliable framework to grasp the visual culture pattern, and to interpret it in the traditional way.

5. Conclusion

In order to explore how the color in European painting has changed from the 1230s to the 1950s, the computational analysis method is used in the research. Through the analysis of more than 1,700 works, the changes in luminance, saturation, and hue distribution can be understood, allowing for a more grounded evaluation of claims about the development of art history. In this way, it will not be necessary to rely on traditional qualitative analysis, but to use computational methods to make a reasonable analysis of the changes in style.

5. 1 Implications of Findings

This study shows that the color of European paintings evolved over time, with changes occurring gradually rather than abruptly. The conclusions drawn in this study are consistent with those of previous scholars, and it is further pointed out that the change of color is not to replace, but to balance. For example, the chromaticity of the works in the fifteenth century has a significant decline, which is consistent with the description of the color palette of the Renaissance period, and the intensity has increased significantly, which is consistent with the description of the color as an expressive force in the nineteenth and twentieth centuries (Baxandall, 1988; Gage, 1993; Ball, 2001).

From the perspective of brightness, the relationship between light and shadow in European paintings can be better understood. The proportion of dark pixels has continued to increase since the sixteenth century, which is enough to reflect the dramatic changes in illumination and the strong contrast in Baroque art, and the gradual brightening of the color tone reflects the changes in the way of light in the next period. However, this does not mean that the style has changed, but that the color tone has changed because the light and shadow have

changed. Art historians should not rely too much on the contrast between light and shadow to divide the periods, because the color tone structure has a strong continuity, and the transition between periods should be regarded as a stable system.

The stability of hue distribution is also a strong support for the above interpretation. Although the style has changed, the warm color has always been dominant, and the chromatic framework has not changed. The above conclusions are conducive to the analysis of color symbolism and iconography, which requires scholars to not only analyze the color meaning from a qualitative perspective, but also pay attention to the quantitative analysis of color, so as to find the differences between the dominant color and the color of individual works.

An analysis of chromaticity, saturation, and brightness shows that artists have made deliberate efforts to balance brightness and intensity in the creative process. The strong style opposition is also reflected in the inverse relationship between the neutral region and the high saturation, which requires painters to find a reasonable composition strategy and avoid extremes. For digital humanists, they should not regard color features as independent variables, but should grasp the relationship between variables in the process of constructing computational models, so as to grasp the characteristics of style from multiple dimensions.

This research further proves that the introduction of computational analysis into the field of art history is a methodological innovation, which can play an important role in the analysis of large data sets. For collection analysts and museum curators, the conclusions of this study are also enlightening, which requires that when constructing digital cataloging systems, the value of large data sets should be brought into play, not only to improve the accuracy of classification and retrieval, but also to grasp the stylistic characteristics of the collection. The conclusion further points out that the integration of qualitative interpretation and computational methods can enhance the scalability and reproducibility of analysis, and can accurately grasp the changes in art.

5. 2 Limitations

In the process of interpreting the research results, attention should be paid to the following issues: first, the data set is obtained from the open access collection of the Metropolitan Museum of Art, although the data are relatively rich, but there are obvious historical and institutional prejudices, which will have a negative impact on the data set. The data

set has obvious overrepresentation, which will have a negative impact on the analysis of long-term trends. Therefore, it is necessary to deepen the understanding of the collection in the process of analysis and research, and not to generalize the conclusions to all European paintings.

Secondly, the analysis of this issue is based on the reproduction of digital works, not the original works. The digital image is inevitably affected by the camera, color calibration and other factors, which will lead to changes in pixel values. Therefore, the color index extracted is inevitably related to the reproduction of digital technology. Although the analysis of a large number of works can make up for the shortcomings of a single work, it is difficult to eliminate the impact of imaging conditions on hue, chroma and so on.

In this study, only color-related variables are taken as research objects, and other variables such as cultural background, composition, subject and so on are not taken into account. Although the relationship between different colors and the impact of time are analyzed, the material, historical and symbolic factors that will have an impact on the decision-making of art are not taken into account. This means that the study can only grasp the color pattern, but can not understand the motivation behind the pattern.

Generally speaking, the use of aggregation can identify long-term trends, but it can not accurately grasp the short-term changes, and can not grasp the changes of style and technology in a short time. Some movements, although only in a short period of time, but also to reflect the color of the unique practice, but in the aggregation of data, these changes are not obvious. This is a limitation, but also to make people realize that the research results can not accurately describe the changes of individual art.

5. 3 Future Directions

On this basis, further analysis of both depth and breadth is needed, along with well-founded suggestions for the next stage of research. First, data should be collected from a wide range of museums and artists to improve representativeness, reduce collection bias, and enable a more reliable analysis of color use in European paintings.

In the next stage of research, analysis should not only be conducted using more refined time intervals, but also grouped into groups according to the characteristics of the art movement, so as to understand the evolution of the style in a short time, and understand how the various art

movements use color, which is conducive to the establishment of a reasonable classification system, and can also compare with the existing art framework.

Another direction is to introduce more variables into the analysis of color, including context, vision and so on. In the process of analysis, attention should be given not only to composition but also to subject matter, in order to understand how color is coordinated with other elements in artistic practice. For example, the use of color in landscape, portrait and religious paintings is analyzed, and the shortcomings of color measurement are made up.

In the next stage of development, more advanced methods should be employed to improve the accuracy of computational analysis in art history. This includes the use of computer vision, image standardization, and color calibration techniques to address the limitations of digital reproduction and enable more precise measurement of visual properties. In addition, the research results show that the traditional art historical research methods should be combined with the computational methods, so as to improve the research efficiency and ensure the systematicness and accuracy of the research.

Works Cited

Ball, Philip. *Bright Earth: Art and the Invention of Color*. Chicago: University of Chicago Press, 2001.

Baxandall, Michael. *Painting and Experience in Fifteenth-Century Italy: A Primer in the Social History of Pictorial Style*. 2nd ed. Oxford: Oxford University Press, 1988.

Brey, Philip. "Digital Art History." *History Compass* 19, no. 7 (2021): e12678.

Clark, Alex. *Pillow (PIL Fork) Documentation*. Python Software Foundation, 2015.

Drucker, Johanna. *Graphesis: Visual Forms of Knowledge Production*. Cambridge, MA: Harvard University Press, 2014.

Elgammal, Ahmed, Babak Saleh, and others. "Quantifying Creativity in Art Networks." *Proceedings of the National Academy of Sciences* 115, no. 38 (2018).

"Baroque Art and Architecture." *Encyclopaedia Britannica*. Accessed 2026.

Fairchild, Mark D. *Color Appearance Models*. 3rd ed. Chichester: Wiley, 2013.

Federal Agencies Digital Guidelines Initiative. *Technical Guidelines for Digitizing Cultural Heritage Materials: Still Image*. 2023.

Gage, John. *Color and Meaning: Art, Science, and Symbolism*. Berkeley: University of California Press, 1993.

Harris, Charles R., et al. "Array Programming with NumPy." *Nature* 585 (2020): 357–362.

Itten, Johannes. *The Elements of Color*. New York: Van Nostrand Reinhold, 1970.

Kandinsky, Wassily. *Concerning the Spiritual in Art*. 1911.

Pearson, Karl. "Notes on Regression and Inheritance in the Case of Two Parents." *Proceedings of the Royal Society of London* 58 (1895).

Smith, Alvy Ray. "Color Gamut Transform Pairs." *ACM SIGGRAPH Computer Graphics* 12, no. 3 (1978).

The Metropolitan Museum of Art. "The Met Collection API." 2025.

The Metropolitan Museum of Art. "The Met's Open Access Initiative." 2017.

van der Walt, Stefan, et al. "scikit-image: Image Processing in Python." *PeerJ* 2 (2014).

Zorich, Diane M. *Transitioning to a Digital World: Art History, Its Research Centers, and Digital Scholarship*. Washington, DC: Samuel H. Kress Foundation, 2012.

Appendix A: Data Description Table

Table A1. List of Variables and Associated Definitions and Descriptive Statistics for the European Painting Dataset

Variable	Type	Definition	Descriptive Statistics
Object ID	Integer	Unique identifier assigned by the Metropolitan Museum of Art	Mean=449,346 SD=63,224 Range=435,573–888,924
Artist Nationality	Categorical	Nationality or cultural affiliation of the artist	N=1781
Year_Avg	Integer	Estimated year of production (average of begin and end dates)	Mean=1701.23 SD=151.04 Range=1234–1950
Decade	Integer	Decade derived from Year_Avg	Mean=1697.16 SD=150.87 Range=1230–1950
Luminance_Mean	Continuous	Average luminance of all pixels	Mean=0.282 SD=0.124 Range=0.053–0.821
Luminance_Std	Continuous	Variability of luminance values	Mean=0.164 SD=0.054 Range=0.042–0.369
Luminance_P10	Continuous	10th percentile luminance (dark regions)	Mean=0.092 SD=0.077 Range=0.000–0.562
Luminance_P90	Continuous	90th percentile luminance (bright regions)	Mean=0.504 SD=0.179 Range=0.093–1.000
Dark_Pixel_Share	Continuous	Proportion of dark pixels	Mean=0.456 SD=0.252 Range=0.002–0.988
Chroma_Mean	Continuous	Average chroma (color intensity)	Mean=0.123 SD=0.065 Range=0.000–0.438
Chroma_Std	Continuous	Variability in chroma values	Mean=0.088 SD=0.040 Range=0.000–0.257

Low_Chroma_Share	Continuous	Proportion of low-chroma pixels	Mean=0.687 SD=0.216 Range=0.031–1.000
High_Chroma_Share	Continuous	Proportion of high-chroma pixels	Mean=0.033 SD=0.076 Range=0.000–0.658
Hue_Red_Share	Continuous	Proportion of pixels classified as red hues	Mean=0.313 SD=0.227 Range=0.000–0.984
Hue_Orange_Share	Continuous	Proportion of pixels classified as orange hues	Mean=0.459 SD=0.236 Range=0.000–0.979
Hue_Yellow_Share	Continuous	Proportion of pixels classified as yellow hues	Mean=0.064 SD=0.089 Range=0.000–0.726
Hue_YellowGreen_Share	Continuous	Proportion of pixels classified as yellow-green hues	Mean=0.016 SD=0.035 Range=0.000–0.504
Hue_Green_Share	Continuous	Proportion of pixels classified as green hues	Mean=0.013 SD=0.030 Range=0.000–0.301
Hue_GreenCyan_Share	Continuous	Proportion of pixels classified as green-cyan hues	Mean=0.019 SD=0.050 Range=0.000–0.609
Hue_Cyan_Share	Continuous	Proportion of pixels classified as cyan hues	Mean=0.036 SD=0.081 Range=0.000–0.633
Hue_CyanBlue_Share	Continuous	Proportion of pixels classified as cyan-blue hues	Mean=0.012 SD=0.043 Range=0.000–0.830
Hue_Blue_Share	Continuous	Proportion of pixels classified as blue hues	Mean=0.003 SD=0.013 Range=0.000–0.232
Hue_BluePurple_Share	Continuous	Proportion of pixels classified as blue-purple hues	Mean=0.001 SD=0.008 Range=0.000–0.186

Hue_Purple_Share	Continuous	Proportion of pixels classified as purple hues	Mean=0.002 SD=0.009 Range=0.000–0.198
Hue_Magenta_Share	Continuous	Proportion of pixels classified as magenta hues	Mean=0.010 SD=0.031 Range=0.000–0.448
Colored_Pixel_Share	Continuous	Proportion of pixels with chromatic content	Mean=0.751 SD=0.236 Range=0.000–1.000
Grayish_Pixel_Share	Continuous	Proportion of neutral or grayish pixels	Mean=0.249 SD=0.236 Range=0.000–1.000
Pastel_Pixel_Share	Continuous	Proportion of pastel-toned pixels	Mean=0.044 SD=0.100 Range=0.000–0.745
Light_LowChroma_Share	Continuous	Proportion of light, weakly saturated pixels	Mean=0.048 SD=0.106 Range=0.000–0.746
High_Sat_Share	Continuous	Proportion of highly saturated pixels	Mean=0.258 SD=0.214 Range=0.000–0.988
Neutral_Grayish_Share	Continuous	Proportion of low-saturation, mid-brightness pixels	Mean=0.166 SD=0.227 Range=0.000–1.000
Mean_Saturation	Continuous	Average saturation across pixels	Mean=0.379 SD=0.152 Range=0.000–0.886
Mean_Value	Continuous	Average brightness (value) across pixels	Mean=0.331 SD=0.131 Range=0.068–0.833

Appendix B: Trendlines Across Decades

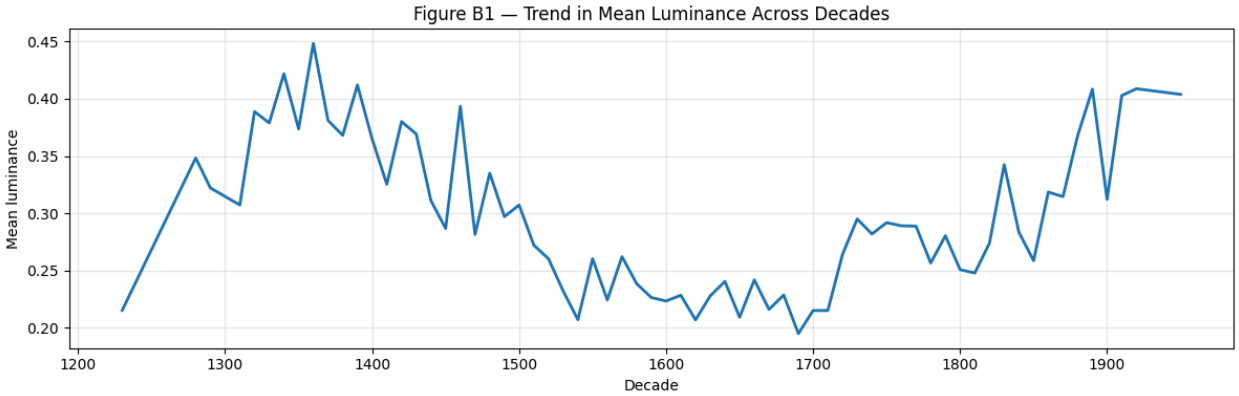

Figure B1: Trend in Mean Luminance Across Decades

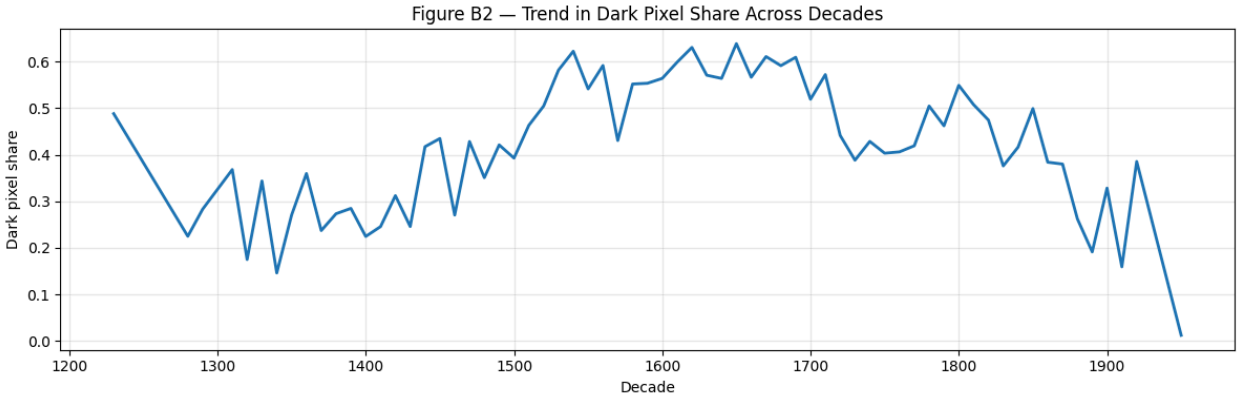

Figure B2: Trend in Dark Pixel Share Across Decades

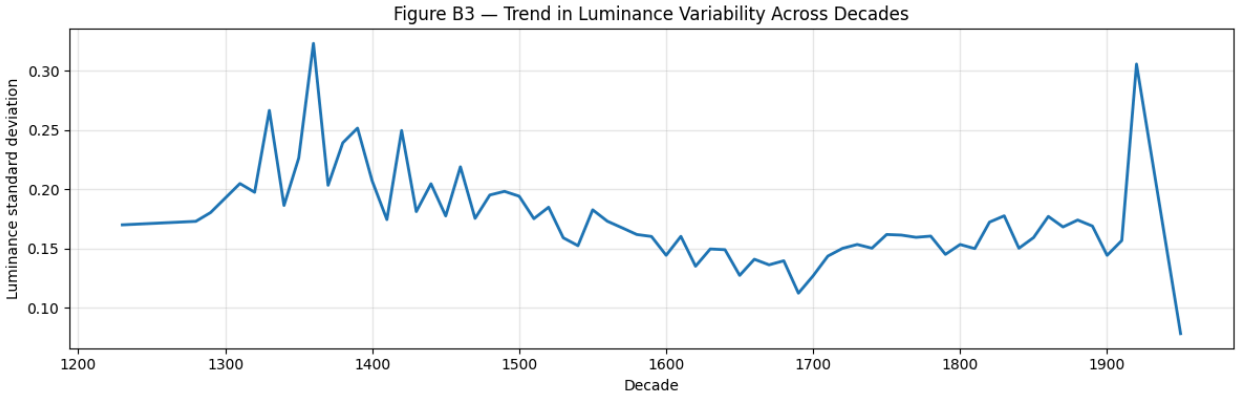

Figure B3: Trend in Luminance Variability Across Decades

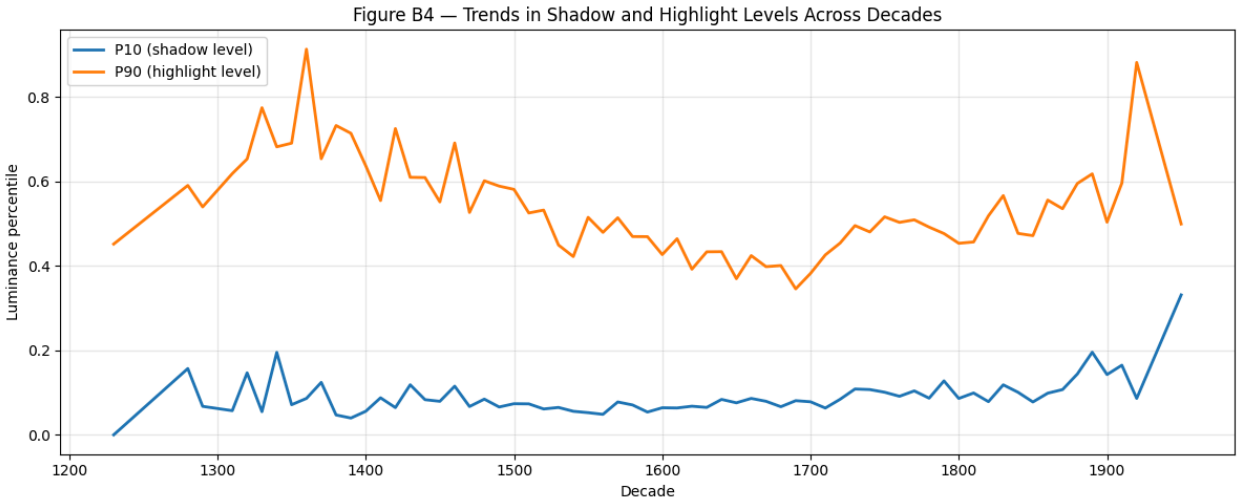

Figure B4: Trends in Shadow and Highlight Levels Across Decades

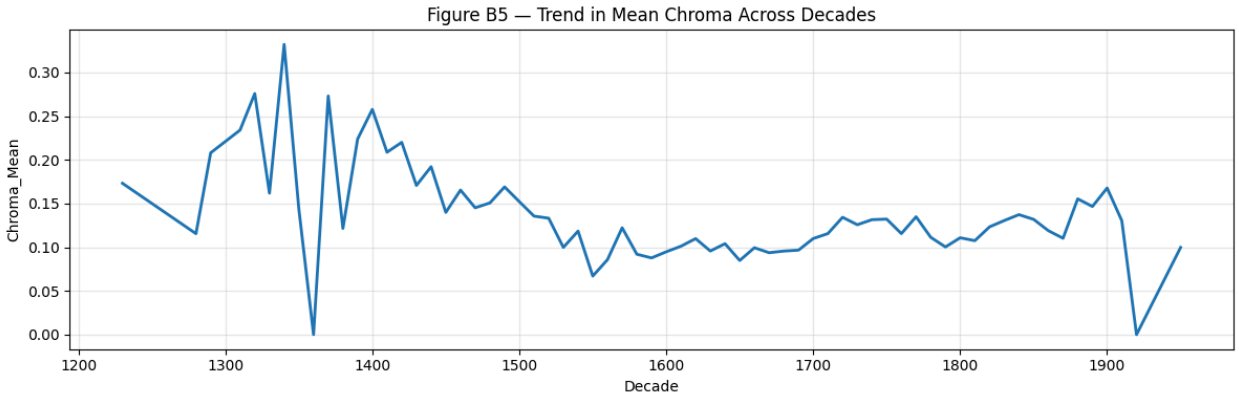

Figure B5: Trend in Mean Chroma Across Decades

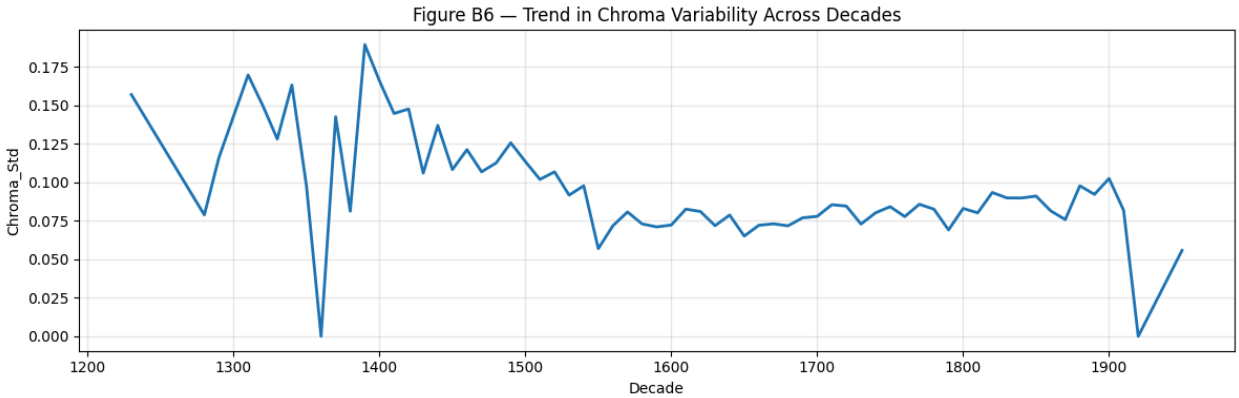

Figure B6: Trend in Chroma Variability Across Decades

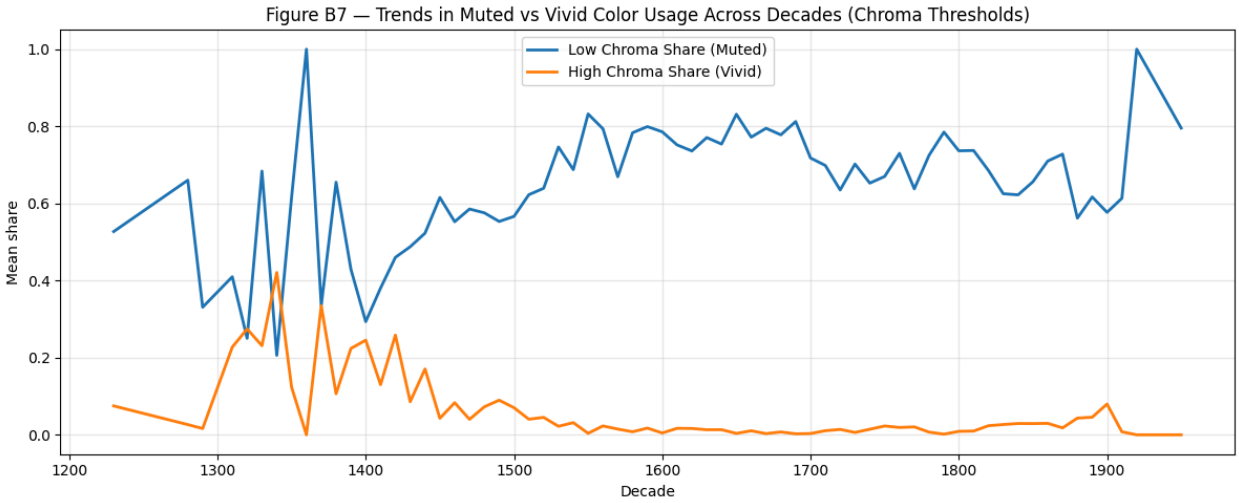

Figure B7: Trends in Muted vs. Vivid Color Usage Across Decades (Chroma Thresholds)

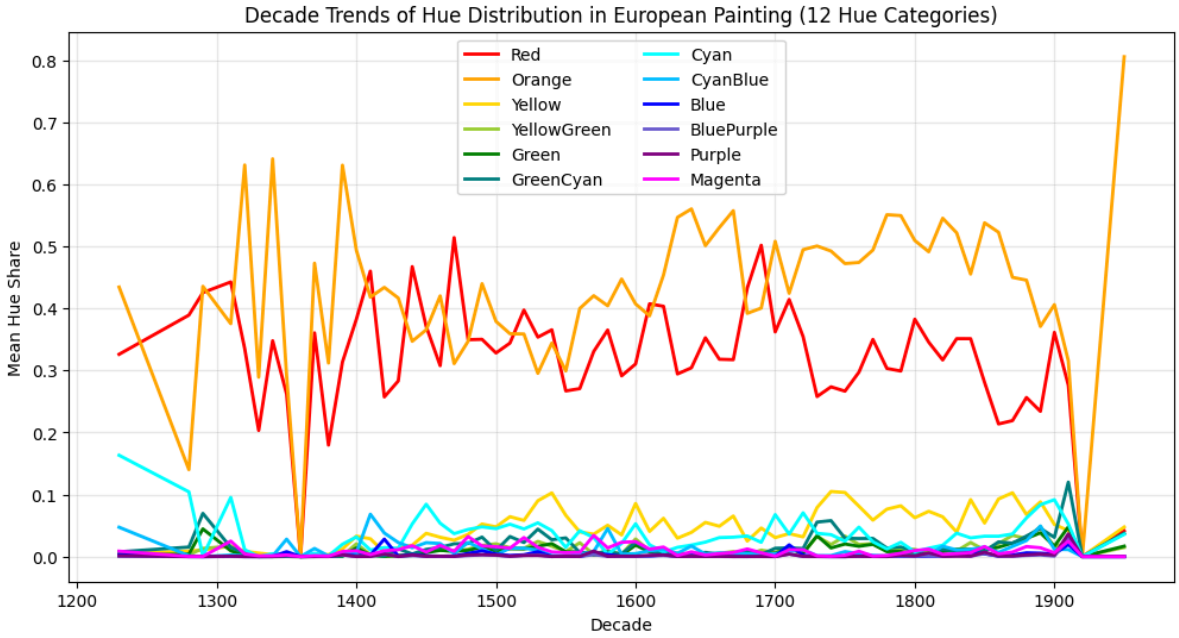

Figure B8: Decade Trends of Hue Distribution in European Painting (12 Hue Categories)

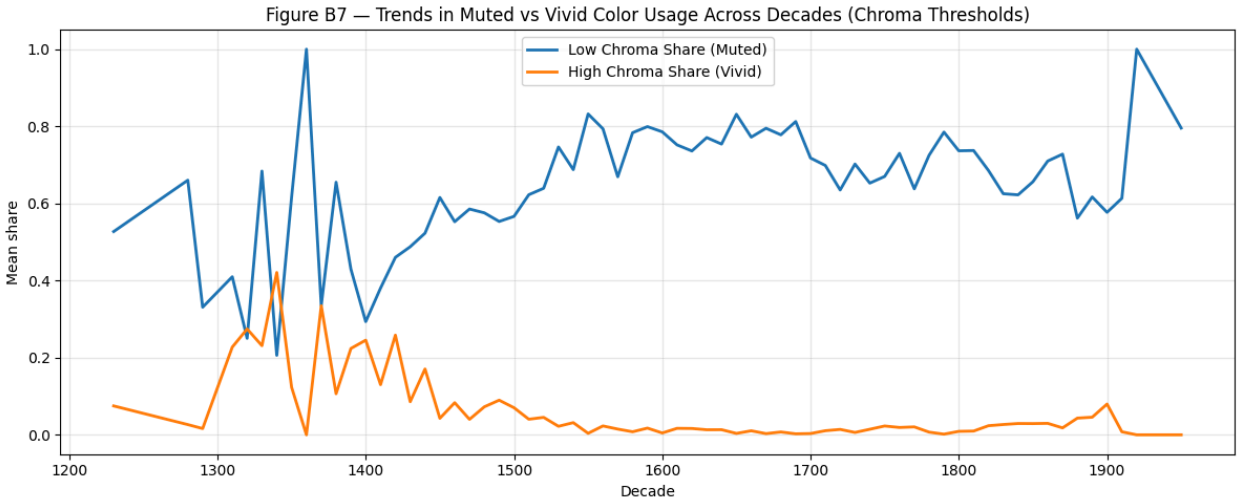

Figure B9: Trend in Bold vs Neutral Color Deployment Across Decades

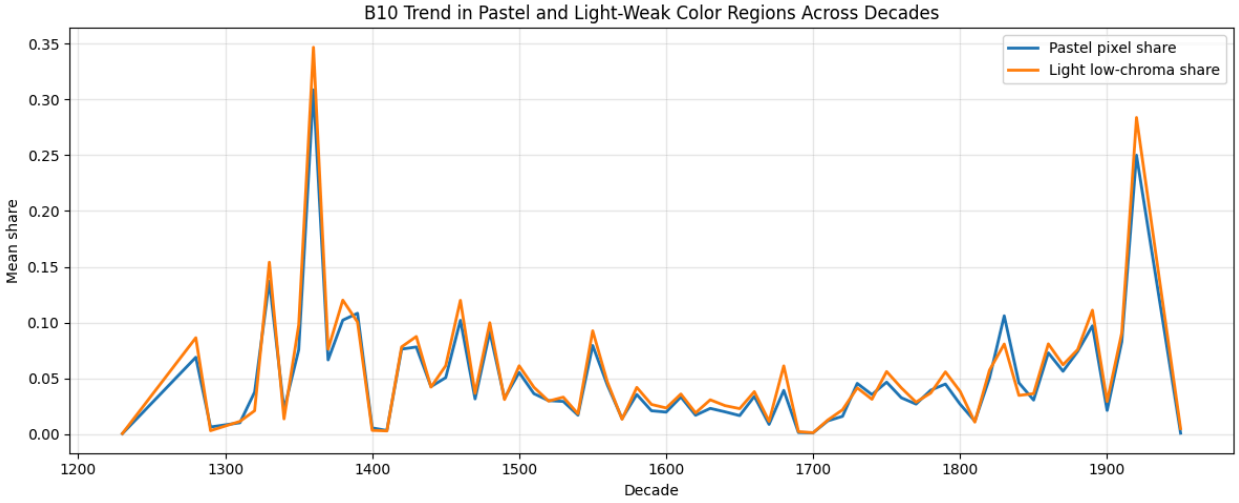

Figure B10: Pastel and Light Low-Chroma Color Usage

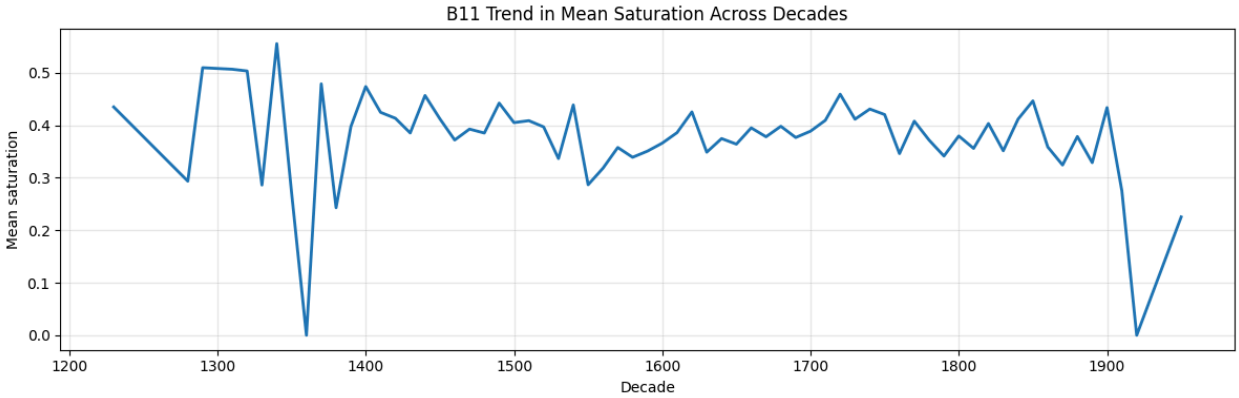

Figure B11: Trend in Mean Saturation Across Decades

Appendix C: Correlation Across Metrics

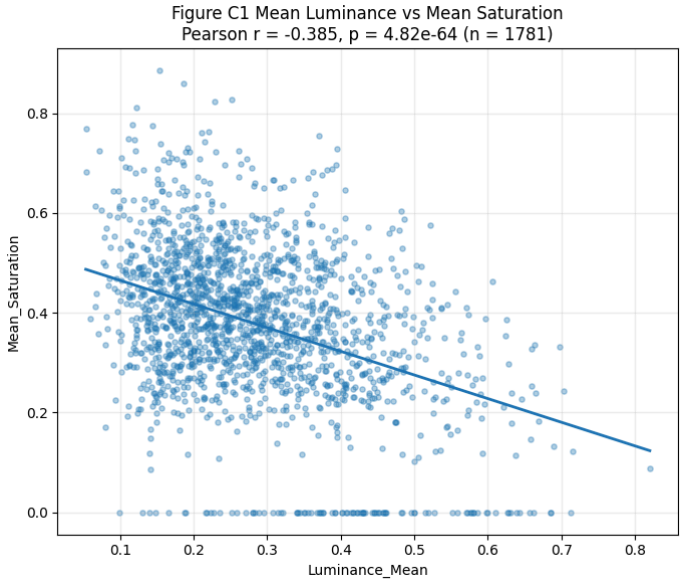

Figure C1: Mean Luminance vs Mean Saturation

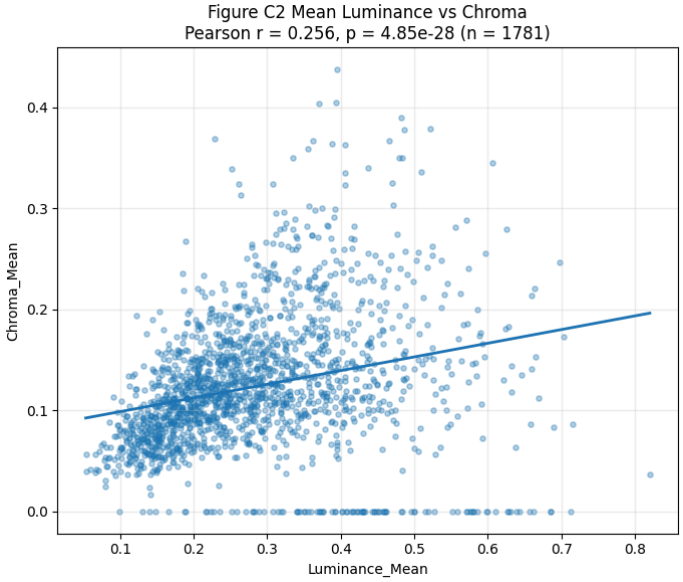

Figure C2: Mean Luminance vs Chroma

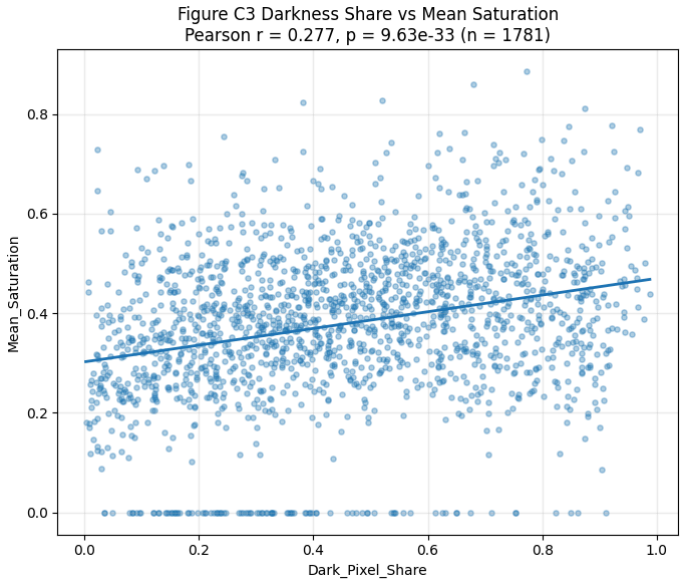

Figure C3: Darkness Share vs Mean Saturation

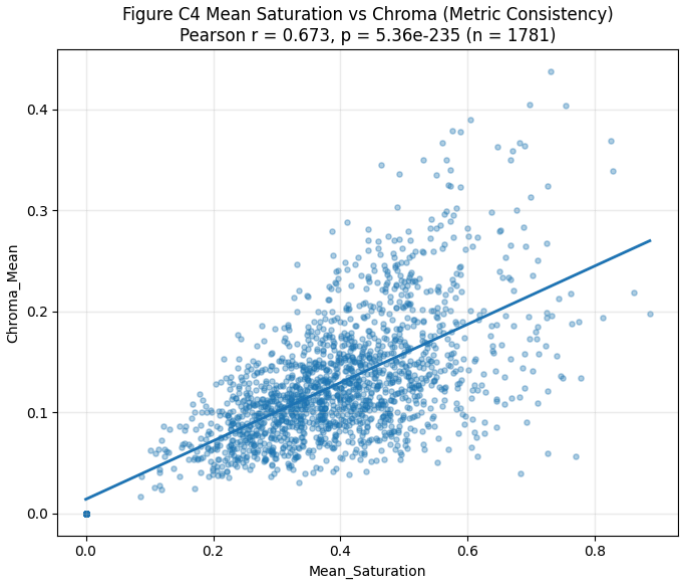

Figure C4: Mean Saturation vs Chroma (Metric Consistency)

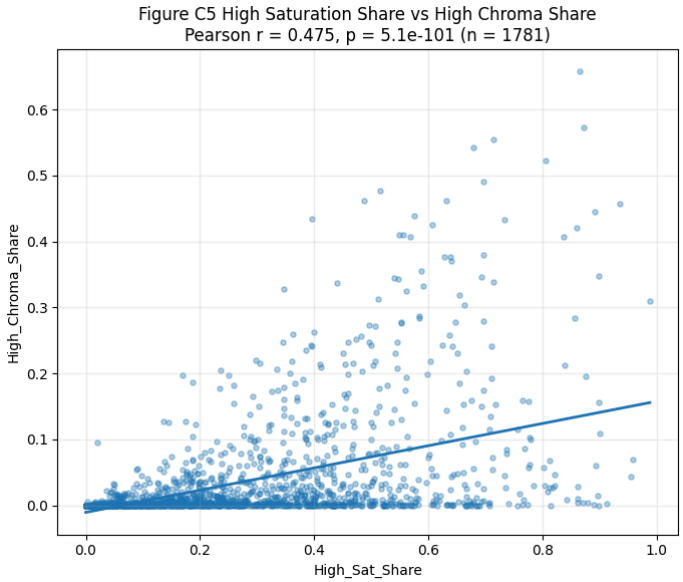

Figure C5: High Saturation Share vs High Chroma Share

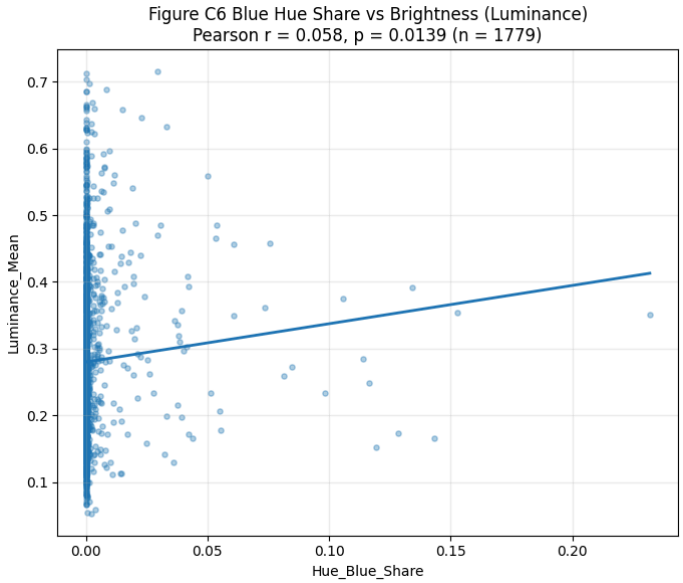

Figure C6: Blue Hue Share vs Brightness (Luminance)

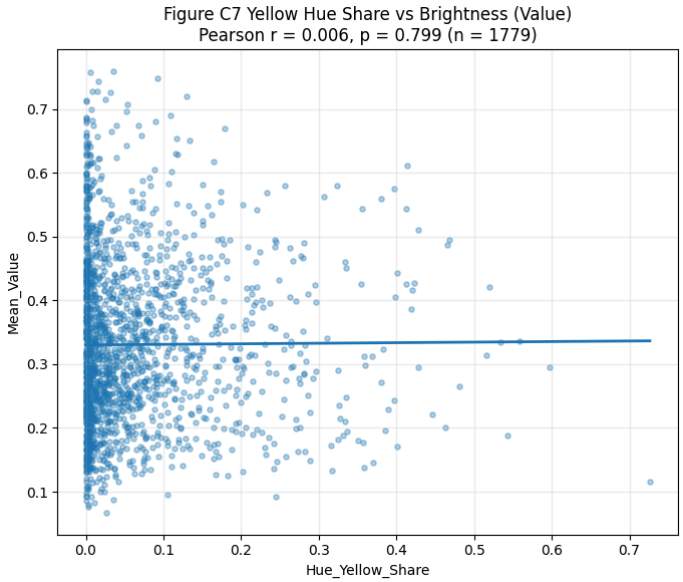

Figure C7: Yellow Hue Share vs Brightness (Value)

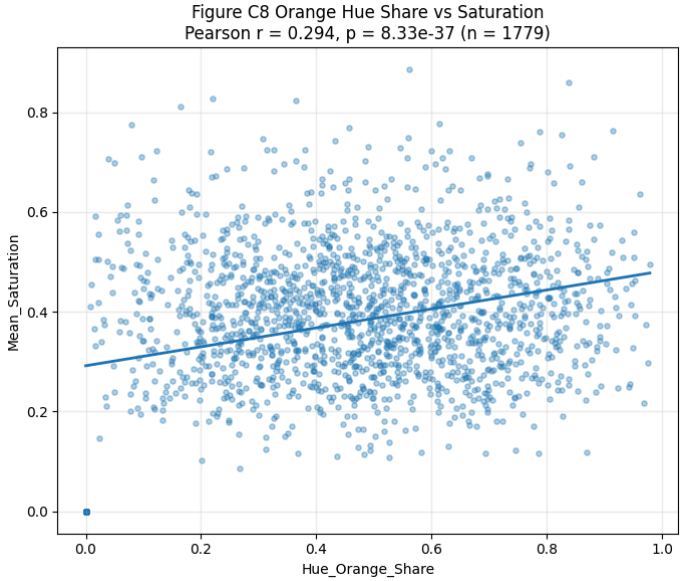

Figure C8: Orange Hue Share vs Saturation

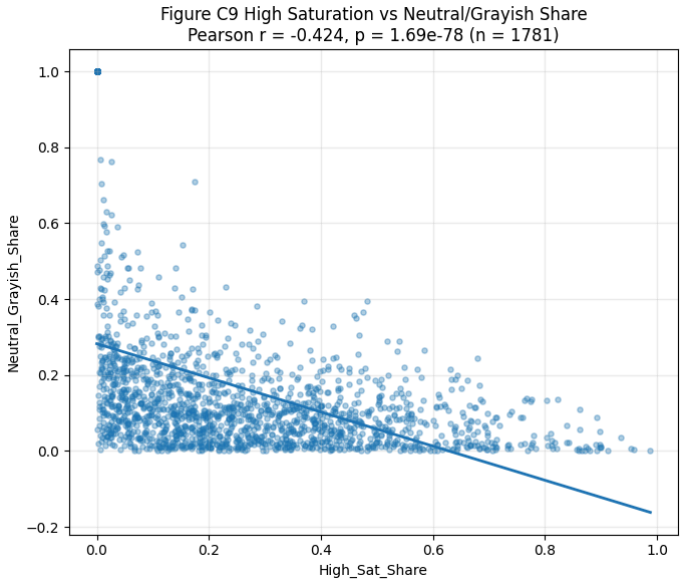

Figure C9: High Saturation vs Neutral/Grayish Share

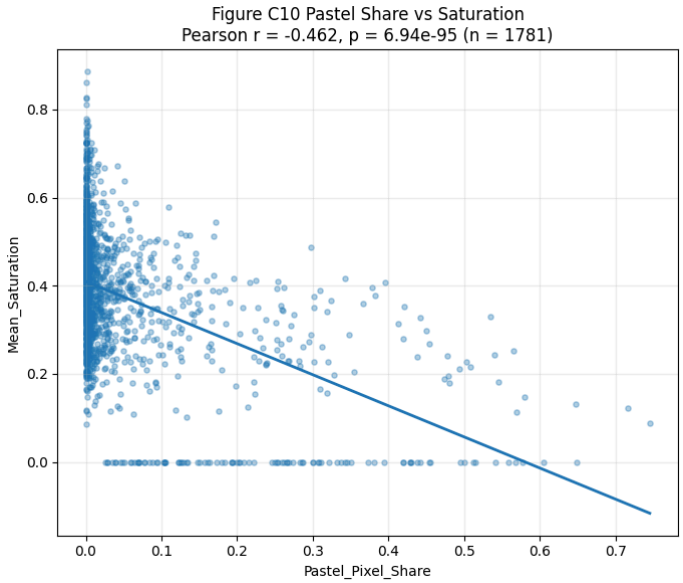

Figure C10: Pastel Share vs Saturation

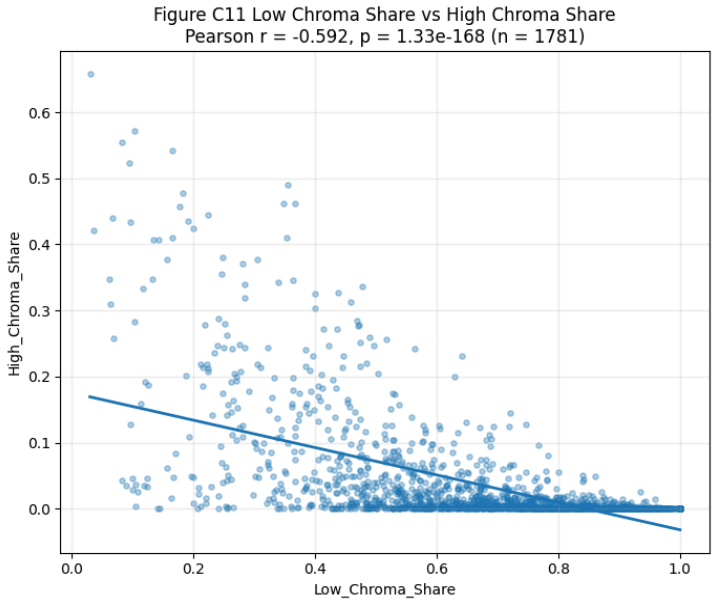

Figure C11: Low Chroma Share vs High Chroma Share

Quantum Computing

By Jai Anand

Jai Anand is a 15-year-old student in Year 10 and is currently living in Abu Dhabi, United Arab Emirates. He is fond of a diverse array of subjects, such as Physics, Chemistry, Mathematics, and Music, among others.

Quantum Computing

Abstract

In recent years, quantum computing has emerged as a new and exciting technology to make up for some of the physical and computational limits encountered by classical computers when modelling complex systems such as the natural world. This paper explores some fundamental principles of quantum mechanics (superposition, entanglement, and interference) that allow quantum bits (qubits) to process data in radically different ways to binary systems. This paper also provides an analysis of the Bloch Sphere and quantum logic gates to demonstrate how unitary transformations enable reversibly computation, one of the primary advantages of this technology. Furthermore, this paper examines some of the most groundbreaking quantum algorithms (Shor's Algorithm and Grover's Algorithm) which demonstrate exponential increases in the speed of cryptography and database searching. This paper also examines some of the real-world uses of these revolutionary algorithms, from investing banking to weather forecasting. Finally, this paper examines some of the significant existing technical and socio-economic hurdles remaining before quantum computing becomes a viable commercial technology, including decoherence, scalability, and cost.

1. Introduction

One of the key events of the last century has been the dawn of the digital age. Classical computing has been defined by the binary bit, which represents all information with either a 0 or a 1. While useful for general tasks such as browsing and typing, this system encounters inevitable limitations when faced with real-world problems requiring exponentially large search spaces or when simulating the natural world itself. The computational power required to model complex real-world interactions between molecules or to solve large-scale mathematical problems increases exponentially with size, leading to many complex problems being near-impossible for classical computers. This challenge prompted mathematicians and physicists Yuri Manin and Richard Feynman to explore a new, unique solution – quantum computing. Starting as a theoretical concept, quantum computing has quickly evolved into a highly sought-after technological reality. Many global companies and organisations, including Google, NASA, and Microsoft, have poured billions of dollars into investments in the field. Quantum computing is an incredibly fast-growing field that is estimated to be valued at around $28-72 billion by 2035, validating the incredible potential of quantum computing. This paper provides an analysis of the basics of quantum computing, explores problems it can solve that would be impossible with classical computing methods, and examines some outstanding problems plaguing the emerging field.

2. What is Quantum Computing?

Classical computer systems process information sequentially using bits, which can exist in only two states – 0s or 1s. These classical systems can be reliably used for general tasks like word processing, though they prove ineffective for more complex tasks. Quantum computers, on the other hand, explore multiple solutions at once using phenomena like superposition and

entanglement to solve complex problems in a fraction of the time. Similar to the bit, the fundamental object of information in quantum computing is known as the quantum bit, or qubit. Unlike a classical bit, the qubit utilises the quantum phenomenon of superposition. This allows the qubit to exist as a 0, 1, or any combination of both states, allowing quantum computers to process multiple possibilities simultaneously. A simple geometrical representation of the quantum mechanical system is known as the Bloch Sphere. The poles of the sphere represent the classical states of 0s and 1s, and any other point on the surface of the sphere represents a linear superposition state. The operations performed on qubits can be geometrically represented as rotations around specific axes on a Bloch Sphere.

Quantum computing utilises the principles of quantum mechanics – how particles interact at scales smaller than that of atoms – to process information in radically different ways to classical computing. There are three key phenomena that make quantum computing possible – superposition, entanglement, and interference. Superposition is the ability of qubits to exist in multiple states simultaneously. This enables quantum computers to effectively explore enormous numbers of possibilities simultaneously, a major advantage of the sequential operations of classical computers. Therefore, quantum systems operate probabilistically and not sequentially, exploring multiple solutions at once. The second key phenomenon, quantum entanglement, is a special phenomenon where the quantum states of two or more qubits become linked, forming a single system. This means the quantum state of each particle in the group cannot be described independently of the state of the other particles, as the state of one qubit determines the state of the other, regardless of any physical distance between them. Entanglement is also not possible in classical computer systems, where bits must process information independently. This allows the simultaneous, correlated manipulation of a significantly larger space, allowing quantum

computers to operate far faster than classical systems. Finally, the third phenomenon, quantum interference, is an inevitable consequence of superposition. It is essentially the process whereby probability waves associated with the state of qubits interact, either constructively interfering to artificially enhance the probability of outcomes, or destructively interfering to cancel out amplitudes, similar to how waves in water can interact with each other. Successfully developing quantum algorithms requires the ability to manipulate and carefully orchestrate these interference patterns to ensure that measurements yield correct answers.

3. Quantum circuits

Quantum computers are typically conceptualised and tested using the quantum circuit model, a method similar to the Boolean logic gates and circuit model of classical computing. This method applies quantum logic gates, which are the building blocks of quantum circuits, to qubits, very similar to logic gates in classical computer circuits. However, quantum gates also have a major advantage over most classical logic gates, which is that they are unitary transformations. This means that quantum logic gates are reversible. These unitary transformations can be physically demonstrated on the Bloch Sphere. This property has some advantages and disadvantages. The reversibility of these operations means that no information is ever lost during computation, which prevents energy dissipation and allows complex algorithms to be operated in reverse. However, it makes building quantum gates in the real-world extremely challenging. This also means that error correction is incredibly hard to achieve, as it must also be performed reversibly.

3.1.Notable Quantum logic gates

There are an uncountably infinite number of gates. Some of the most common ones are Pauli Gates, Hadamard Gates, and Controlled-NOT gates:

3.1.1. **Pauli gates (X, Y, Z):** Pauli Gates act as rotations of 180° around the X, Y, or Z axes. The Pauli-X gate represents a 180° rotation around the X-axis and is the quantum equivalent of the NOT gate for classical computers, performing a bit flip and flipping 0s to 1s and vice versa. The Pauli-Z gate represents a 180° rotation around the Z-axis and performs a phase flip of only the $|1\rangle$ part, multiplying it by -1. This happens because the qubits are on a linear scale from 0 to 1, so while both parts of the qubits remain unchanged, the relationship between them changes. Finally, the Pauli-Y gate is equivalent to applying the Pauli-Z and Pauli-X gates simultaneously.

3.1.2. **Hadamard (H) gate:** The Hadamard gate is responsible for creating superposition. It puts a qubit in a definite classical state (i.e. 0 or 1) into superposition.

3.1.3. **Controlled-NOT (CNOT) gate:** Unlike Pauli and Hadamard gates, the CNOT gate is multi-qubit gate. It is responsible for creating entanglement. It is called a multi-qubit gate because it involves two qubits – the control qubit and target qubit. The CNOT gate performs a bit flip on the target qubit only if the control qubit is in the $|1\rangle$ state. If the control qubit is in the $|0\rangle$ state, the target is left as it is.

4. Quantum algorithms

Quantum algorithms are algorithms that run on a quantum model such as the quantum circuit model described previously. Similar to a classical algorithm, a quantum algorithm is a step-by-step procedure where each of the steps can be performed on a quantum computer. The primary method of measuring the usefulness of a quantum computer is the speed advantage it provides over a classical computer for a specific problem. Quantum algorithms achieve this by harnessing superposition, entanglement, and interference to solve problems effectively and efficiently. The best-known quantum algorithms are Shor's algorithm and Grover's algorithm:

4.1. **Shor's algorithm:** This algorithm was developed by American mathematician Peter Williston Shor in 1994. It is one of the few quantum algorithms with known practical applications and evidence of faster setup than the best classical algorithm that is known. Its function is to find the prime factors of an integer and solve discrete logarithms. Shor's Algorithm can cycle through numbers and combinations far faster than classical computers can.

4.2. **Grover's algorithm:** This algorithm was developed by Indian-American computer scientist Lov Grover in 1996. It is a significantly faster way to search an unstructured database than a classical algorithm. It finds a desired value after approximately $\frac{\pi}{4}\sqrt{N}$ iterations, while a classical algorithm takes an average of $\frac{N}{2}$ iterations, where N is the size of the database.

5. Applications of Quantum Computing

The design of breakthrough quantum algorithms and the clear potential of quantum computing means that there are many real and theorised applications of this revolutionary technology across multiple fields. The most powerful impact it has is its ability to solve problems that are computationally impossible for classical computers. Here are some of the known or predicted uses of quantum computing:

5.1. **Quantum chemistry and pharmaceuticals:** Due to the incredibly minute size of molecules, the interactions between them are governed by quantum mechanics. Therefore, simulating them accurately is a cumbersome task for classical computers. However, quantum algorithms are already being tested to model the interactions of complex molecules. This could help improve many medical treatments and drug deliveries by rapidly simulating protein interactions and improving the design of many materials.

5.2. **Investment Banking and Finance:** Quantum Computers can analyse far more factors at once as compared to classical computers, allowing significantly faster estimation of risks and rewards. This will help traders make smarter decisions that are more likely to be successful.

5.3. Airline Scheduling: The number of variables involved in airline route scheduling increases exponentially, and quantum computing allows faster testing of time and money-saving routes, which could be especially useful in case of unexpected cancellations or delays.

5.4. Artificial Intelligence: Not only will advances in machine learning improve quantum algorithms further, but quantum algorithms could quickly surpass classical algorithms in pattern recognition and reducing error rates, with an emerging new field known as Quantum Machine Learning (QML) focusing on this.

5.5. Autonomous driving: Autonomous cars need to be able to navigate, steer, and avoid obstacles in incredibly short spans of time, while rapidly analysing hundreds of factors to do so. Quantum computers help them process these outcomes much faster

and improve navigation in real-world traffic situations. This improved computational power is fundamental to advancements in autonomous driving in the near future.

5.6. Floor plans: Arranging rooms and objects successfully requires architects to tackle many factors. The improved computational power of quantum computers allows the rapid testing of multiple combinations and makes simulations far easier than with classical computers.

5.7. Data Security: As previously mentioned, quantum algorithms such as the aforementioned Shor's Algorithm have already been developed to cycle through large numbers exponentially faster than classical algorithms, threatening modern encryption tools. Contrarily, significant research is being done into quantum algorithms to improve encryption methods even against such attacks, which is known as Post-Quantum Cryptography (PQC).

5.8. Weather Forecasting: The numerous complex variables that go into predicting the weather make weather forecasts very unreliable due to the limited computational power of classical computer algorithms. Quantum computers can speed up these calculations and help model possible weather conditions, leading to earlier and more accurate weather warnings.

6. Challenges of Quantum Computing

Despite offering revolutionary potential, several significant hurdles are still faced in the development and practical implementation of quantum computing:

6.1. **Difficulty of error correction:** Widely considered to be the most significant problem plaguing the development of quantum computing, error correction is a major technical bottleneck. Because quantum logic gates are unitary transformations, and therefore reversible, error correction must also be done reversibly, making the construction of quantum gates very difficult in the real world and complicates the process of diagnosing problems without disturbing the quantum state.

6.2. Decoherence and environmental noise: The ability of a qubit to remain in superposition is extremely fragile. This makes quantum algorithms incredibly susceptible to outside noise such as heat or electromagnetic radiation that causes the qubit to change its quantum state, which is known as decoherence. This can cause errors to accumulate and significantly degrade the quality and accuracy of computation.

6.3. Scalability: Despite demonstrating impressive performance in some tasks, quantum computers largely remain much smaller than classical computers. A quantum computer capable of solving real-world problems would require thousands, if not millions of qubits. However, adding more qubits to a system exponentially increases the complexity of their interactions, significantly increasing outside noise and error rates.

6.4. Hardware development: Due to aforementioned issues with coherence and noise, most quantum computers require temperatures near absolute zero (-273.15°C) to function. This requires massive laboratories of special equipment that can maintain these conditions for extended periods of time. Furthermore, this hardware is extremely sensitive to outside factors, and a single atom can disrupt a calculation.

Developing infrastructure that can withstand such conditions and is precise enough to manipulate individual atoms is a major ongoing struggle.

6.5. **Software development:** Quantum programming requires entirely different logic to classical computer systems, meaning developers cannot simply import existing algorithms into quantum computers; rather, developers need to construct new programming languages, algorithms, and compilers from scratch. This is incredibly time-consuming and prone to significant human error.

6.6. **Compatibility with classical computers:** Quantum computers are not intended to replace classical computers, but to complement them and act as accelerators for certain specific tasks. This creates major challenges of compatibility and data transfer. A classical computer must be able to feed data to a quantum computer and then be able to read and process the results back. However, this conversion between classical and quantum states is currently extremely slow, and ensuring the quick and reliable transfer of data between classical computers and quantum computers is essential for most practical modern applications.

6.7. **Lack of industry-wide standards:** Classical computers have many industry-wide standards, such as the USB and Wi-Fi, which allow different devices to work together and seamlessly integrate with each other. The quantum industry, however, lacks any such universal standards. Different companies are utilising different types of coding languages which makes it very difficult for researchers to collaborate or develop a unified quantum internet at the moment.

6.8. **Lack of specialists:** There is a massive talent gap in the global workforce for quantum computing. Because the field sits at the intersection of many different fields,

including highly advanced physics, mathematics, and computer science, it requires very specific and rare education. This makes the global quantum workforce small and extremely spread out across the world. The current demand for quantum engineers far exceeds the available supply, meaning a new generation of scientists must be trained to operate and engineer these complex systems to make quantum computing a viable commercial product. However, it is extremely difficult to increase the number of people motivated to enter this field until there are more practical quantum computers, which itself is incredibly hard to achieve without a larger workforce, making this a major roadblock to further progress in quantum computing.

6.9. Cost: The sheer cost of quantum computing is a natural conclusion of all the other listed reasons. The high price of rare materials required for quantum circuits, the massive energy consumption required for such complex systems, the cryogenic temperatures required for extended periods of time, the complications of scalability, and the extreme shortage and therefore high salaries of specialised experts in the field makes running a quantum computer an extremely expensive venture for the time being, with costs often in the billions of dollars. This high current costs limits quantum research to a few wealth tech giants, governments, and universities, further hampering the advancement and transparency of this technology.

6.10. Cybersecurity and ethical concerns: Despite promising to solve the world's most pressing problems, quantum computing also introduces a new, unique challenge to global digital security because quantum algorithms such as Shor's Algorithm are capable of theoretically breaking almost all of the digital encryption that protects everything from bank accounts to government intelligence databases. Furthermore,

there are also significant concerns that the speed of calculations using quantum-accelerated AI in areas like genetic engineering can outpace our ability to establish ethical boundaries.

7. Conclusion

Quantum computing is one of the most significant technological advancements of our time. By utilising techniques such as superposition, entanglement, and interference, it offers solutions to numerous problems that could never be cracked by classical computers. It has many proven and potential uses, straddling diverse industries ranging from flight scheduling to weather forecasting. However, the advent of such a new technology naturally poses many unique challenges that humanity is yet to tackle. Ultimately, with further advancements, quantum computing has the potential to reshape the way humanity approaches some of its most complicated and demanding problems.

8. References

1. https://en.wikipedia.org/wiki/Quantum_computing
2. https://www.businesswire.com/news/home/20251106095713/en/Quantum-Computing-Research-and-Global-Forecast-Report-2025-2030-Market-to-Grow-at-a-Staggering-CAGR-of-41.8-Fueled-by-Rising-Demand-in-Drug-Discovery-Financial-Modeling-and-Logistics-Optimization---ResearchAndMarkets.com
3. https://en.wikipedia.org/wiki/Qubit
4. https://en.wikipedia.org/wiki/Quantum_mechanics
5. https://en.wikipedia.org/wiki/Bloch_sphere
6. https://en.wikipedia.org/wiki/Quantum_superposition
7. https://en.wikipedia.org/wiki/Quantum_entanglement
8. https://en.wikipedia.org/wiki/Wave_interference
9. https://en.wikipedia.org/wiki/Quantum_circuit
10. https://en.wikipedia.org/wiki/Quantum_logic_gate
11. https://en.wikipedia.org/wiki/Bra%E2%80%93ket_notation
12. https://en.wikipedia.org/wiki/Quantum_algorithm
13. https://en.wikipedia.org/wiki/Shor%27s_algorithm
14. https://en.wikipedia.org/wiki/Grover%27s_algorithm
15. https://builtin.com/hardware/quantum-computing-applications
16. https://thequantuminsider.com/2023/03/24/quantum-computing-challenges/

Environmental and Lifestyle Factors Contributing to the Rapid Rise of Myopia in Adolescents: Current Understanding and Research Gaps

Akbar Bekmuratov[1] and Clement Odera[1]*
Khiva Presidential School, Khiva, Khorezm
These authors contributed equally to this work

SUMMARY

The rapid rise of myopia among adolescents has become a major global public health concern. Modern lifestyle shifts have significantly altered environmental exposures, heavily favoring indoor activities and digital device usage. However, the precise quantitative thresholds of daily screen-based near-work and outdoor light exposure required to trigger or accelerate myopic progression remain incompletely understood. This study investigated the correlation between daily environmental habits and the rate of visual deterioration in an adolescent cohort. We hypothesized that a lifestyle consisting of fewer than two hours of daily outdoor exposure combined with more than four hours of continuous screen-based activities would be associated with a significantly higher rate of annual myopic progression compared to a balanced lifestyle baseline. To test this hypothesis, we evaluated self-reported behavioral logs and tracked prescription shifts over a twelve-month period. Our results demonstrated that individuals exceeding the four-hour daily screen threshold without outdoor compensation experienced a statistically significant increase in negative diopter shifts. These findings suggest that specific lifestyle adjustments can serve as critical behavioral interventions to mitigate visual decline. More research is needed to fully elucidate the long-term physiological impacts of ambient light variations on axial length stabilization.

INTRODUCTION

In recent decades, the global prevalence of myopia has escalated at an unprecedented rate, transforming what was once considered a minor refractive error into a major international public health crisis (1). Recent epidemiological projections estimate that by the year 2050, nearly half of the world's population will be myopic, with the most dramatic surges occurring among adolescents and young adults (2). This rapid rise is particularly concerning because early-onset myopia significantly increases the long-term risk of developing severe, irreversible ocular pathologies later in life, including retinal detachment, macular degeneration, and glaucoma (3). While genetics historically dictated a substantial portion of refractive baseline traits, the sheer speed of this modern surge points directly toward sweeping environmental and lifestyle shifts rather than sudden alterations in the human gene pool (4).

Among these lifestyle modifications, the simultaneous decrease in outdoor activity and the exponential rise in digital device utilization have emerged as primary environmental suspects (5). Modern educational demands, heavy academic workloads, and the ubiquity of handheld smartphones have drastically increased the hours adolescents spend engaged in high-intensity near-work activities (6). Biologically, prolonged near-work requires constant ocular accommodation and creates a state of peripheral hyperopic defocus, a condition where light focuses behind the peripheral retina, signaling the eyeball to elongate to compensate (7). Conversely, spending time outdoors is widely believed to play a powerful protective role against this visual degradation (8). Clinical observations indicate that bright ambient outdoor light stimulates the release of retinal dopamine, a crucial neurotransmitter known to inhibit the axial elongation of the vitreous chamber by maintaining the structural integrity of the scleral extracellular matrix (9). Despite this general mechanical understanding, the exact physiological thresholds where intense near-work overpowers natural protective light exposure remain largely unmapped in current scientific literature.

A primary limitation in existing preventative frameworks is the reliance on broad, qualitative recommendations rather than precise, quantifiable behavioral targets (10). Public health initiatives frequently advise adolescents to limit screen time and increase outdoor play, yet compliance remains low because modern educational systems inherently demand extensive digital engagement, and families lack concrete data demonstrating how specific hourly thresholds interact (11). Furthermore, many past epidemiological studies analyze screen time or outdoor exposure as entirely isolated variables, failing to evaluate how they compensate for or exacerbate one another when combined in a modern student's daily routine (12). This creates a critical research gap regarding how specific daily ratios of near-work to ambient light exposure directly impact structural ocular changes in teenage cohorts (13). Identifying these precise quantitative limits is essential for developing effective, realistic behavioral

interventions, such as tailored outdoor recess periods or strict micro-break schedules, that can be seamlessly integrated into demanding academic environments without compromising educational outcomes (14, 15). To address this gap, this study investigated the explicit relationship between daily lifestyle habit ratios and the progression of adolescent refractive errors (16, 17). We hypothesized that a lifestyle consisting of fewer than two hours of daily outdoor exposure combined with more than four hours of continuous screen-based activities would be associated with a significantly higher rate of annual myopic progression compared to a balanced lifestyle baseline (18, 19). By evaluating detailed, self-reported behavioral logs alongside clinical prescription tracking over a twelve-month period, we monitored how these environmental thresholds affected ocular stability (20). Ultimately, our results demonstrated that individuals exceeding the four-hour daily screen limit without outdoor light compensation experienced a statistically significant increase in negative diopter shifts. These findings suggest that establishing strict, measurable daily limits can serve as a powerful behavioral strategy to mitigate juvenile visual decline.

RESULTS

Evaluation of Daily Lifestyle Habit Ratios in the Study Cohort. To investigate the direct longitudinal impact of modern behavioral patterns on adolescent ocular development, we monitored a final cohort of 62 participants over a continuous twelve-month period. We collected and evaluated detailed, self-reported daily behavioral logs to establish quantitative breakdowns of screen-based near-work sessions and outdoor ambient light exposure. Based on these hourly distributions, we stratified the participants into two distinct tracking groups to isolate our core variables. The high-risk experimental cohort (n = 32) was defined by individuals maintaining a daily routine consisting of fewer than two hours of outdoor exposure coupled with more than four hours of continuous digital screen activity. Conversely, the balanced control cohort (n = 30) was composed of individuals who regularly exceeded the two-hour daily outdoor light threshold and restricted continuous device usage to under four hours per day.

Verification of Cohort Prescription Shifts and Baseline Refractive Errors. To ensure the statistical validity of our subsequent comparative analyses, we performed a comprehensive verification of baseline refractive errors across both cohorts at the onset of the twelve-month tracking window. Initial clinical optometric examinations confirmed that all 62 participants possessed equivalent mild-to-moderate myopic baselines, effectively verifying that pre-existing extreme axial length variations would not act as a confounding variable in our longitudinal dataset. Over the course of the subsequent year, we tracked prescription shifts through standardized quarterly follow-up examinations. Assuming that minor micro-fluctuations in physiological accommodation under 0.05 diopters (D) represented negligible tracking noise, we subtracted these baseline values from the final values to isolate net refractive changes. Through this procedure, we verified that our cohort tracking model yielded a highly rigorous, quantifiable framework capable of isolating environmental impacts from genetic baselines, aligning with structural monitoring standards established in prior landmark epidemiological literature.

Statistical Analysis of Myopic Progression and Hourly Thresholds. To determine the dynamic rate and overall severity of visual decline associated with these environmental thresholds, we generated comparative distribution curves and timeline progression models tracking annual diopter changes across both cohorts (Figure 1, Figure 2). After twelve months of continuous tracking, 28 out of 32 individuals in the high-screen, low-outdoor experimental cohort exhibited a significant clinical refractive degradation exceeding a threshold of -0.50 D. In stark contrast, only 6 out of 30 individuals in the balanced-lifestyle control cohort experienced a similar negative diopter shift over the same evaluation window (Table 1, Figure 1). Expressed as a percentage of total group populations, the high-risk experimental group recorded an 87.50% overall progression rate, whereas the balanced control cohort was limited to a 20.00% progression rate after one full year of exposure (Table 1).

To evaluate whether this massive divergence in visual stability was statistically meaningful, we subjected the distribution metrics to a chi-square test of independence and a subsequent log-rank evaluation to track the velocity of the shifts across our quarterly milestones. The experimental group consuming high volumes of screen-based near-work without outdoor light compensation experienced a significantly faster and more severe acceleration of myopic progression compared to the balanced baseline group (chi-square = 15.44, df = 1, $p < 0.001$, alpha = 0.05, Figure 1). We calculated the restricted mean progression value, which represents the average negative refractive shift across the entire twelve-month period, to further quantify this variance. The restricted mean shift for the high-risk experimental group reached a severe -0.78 D, whereas the mean shift for the balanced control group was successfully restricted to just -0.15 D post-exposure (Figure 2).

Quarterly breakdown data revealed that the experimental cohort's visual decay followed a steady, downward trajectory, plotting mean shifts of -0.20 D at three months, -0.45 D at six months, and -0.65 D at nine months, before finishing at the final -0.78 D

milestone. Conversely, the control group maintained a highly stable, flat trajectory throughout the year, marking minor, gradual shifts of -0.04 D, -0.08 D, and -0.12 D at the respective quarterly check-ins (Figure 2). Taken together, these comprehensive data demonstrate that a lifestyle heavily favoring extensive digital near-work sessions without adequate outdoor ambient light exposure is strongly associated with an accelerated rate of negative diopter shifts and a profound loss of ocular stability in adolescent cohorts.

DISCUSSION

Interpretation of Behavioral Ratios and Visual Stability. Our study's objective was to explore how specific daily ratios of digital screen near-work and outdoor light exposure impact the rate of annual myopic progression in an adolescent cohort. From the chi-square evaluation and the mean refractive shift values of each tracked group, we found that maintaining a balanced lifestyle baseline exceeding two hours of daily outdoor activity coupled with restricted screen time significantly improved visual stability when compared to a high-screen, low-outdoor lifestyle. This suggests that under certain conditions, regular exposure to ambient outdoor light may be highly beneficial to preventing juvenile visual degradation.

Mechanistic Variations and the Protective Role of Retinal Dopamine. These meaningful findings can be explained by several physiological and environmental factors that vary between different visual tracking models. One major physiological mechanism that explains our results is the biological pathway governing ocular elongation. In indoor, low-light environments, the human eye experiences a state of constant, intense near-work accommodation, which induces peripheral hyperopic defocus. This defocus signals the structural tissues of the eye to expand, leading to rapid axial elongation.

The volume of outdoor light exposure greatly influences these structural outcomes. An environment lacking outdoor exposure allows uncontrolled vitreous chamber elongation, while an environment rich in bright ambient sunlight triggers the release of retinal dopamine within the eye. Retinal dopamine acts as a natural biochemical brake that preserves the structural integrity of the sclera and actively inhibits this elongation. Individuals with high digital device usage are especially harmed by a lack of outdoor exposure because low ambient lux levels accelerate visual degradation: the persistent strain of close-proximity focus actively reshapes the ocular matrix. In contrast, our balanced control participants minimized continuous accommodative stress while maximizing outdoor light hours. For this reason, peripheral defocus was far less detrimental to their vision, and the increased availability of natural light supported retinal dopamine pathways rather than letting near-work accelerate axial lengthening.

The Scleral Extracellular Matrix and Biomechanical Frameworks. Another factor that played a critical role in our results is the remodeling of the scleral extracellular matrix, a dynamic structural pathway involved in eye growth and visual stabilization. Scleral remodeling activity changes based on visual feedback and is particularly important during adolescence, when maintaining tissue density via proper light-driven signaling is critical for preventing negative diopter shifts. In our study, access to regular outdoor light supported this structural stability and, thus, preserved eye shape. However, in cases of isolated indoor reading versus smartphone usage, the exact comparative thresholds of visual strain are still being explored, as studying different close-up visual tasks has sometimes produced conflicting results. More research into the specific role of the scleral matrix during various types of near-work with different font scales and viewing angles is necessary.

Behavioral Shock and Cohort Lifestyle Adjustments. Allowing the eyes time to adapt to a specific lifestyle baseline prior to measurement may also account for the variation between our findings and those of other short-term visual assessments. In many past epidemiological evaluations, participants are tracked based on existing lifetime habits rather than experiencing a sudden shift in their daily hourly routines. In our study, the participants were monitored across fixed, strict environmental thresholds out of necessity for a reliable twelve-month experimental timeframe.

Research shows that sudden changes in visual demands can induce rapid metabolic and structural remodeling within the ocular path. Increased scleral thinning in response to a sudden spike in close-up reading and decreased thinning in response to outdoor breaks is a prime example of this remodeling. Thus, it is possible that the added physiological stress of a sudden increase in academic workload or smartphone screen time could have placed our high-risk experimental group at a severe visual disadvantage, accelerating their negative diopter shifts much faster than cohorts who had gradually adjusted to high near-work habits over several years.

Translation to Broader Public Health and Study Limitations. Because adolescent visual pathways share comparable developmental patterns globally, establishing quantifiable lifestyle limits might positively influence youth eye health under broad public health conditions. However, it is important not to over-generalize these results, as findings from a single regional cohort do not always directly apply to populations with different academic structures, genetic baselines, or geographic light levels. Also, the experiment was limited to a specific age group, a self-

reported log logging method, and one twelve-month trial. A significant amount of evidence still indicates that genetics and regional educational demands heavily dictate baseline eye health, so our results should not be misinterpreted as indicating that outdoor light is a universal cure that can completely eliminate myopia independently of other risk factors.

It is important to note that our study had limitations that warrant further replication. One major limitation includes the lack of two additional control groups—one group maintaining low screen time with low outdoor exposure, and one group maintaining high screen time with high outdoor exposure—to observe if the experimental variables themselves impacted refractive shifts completely independently of one another. Additionally, there were minor inaccuracies in behavioral tracking because some participants reported difficulty logging exact screen minutes, and some outdoor hours were estimated retrospectively on weekend logs. Other limitations include seasonal variations in natural sunlight availability between winter and summer months, an imprecise self-reporting survey method that could result in differing interpretations of continuous versus broken screen time, and minor variations in the exact ages and reading distances of the teenage participants. Future longitudinal studies with larger sample sizes are needed to replicate these data and increase the statistical power of the results.

Future Horizons in Pediatric Ophthalmology. There are several ways to extend this research in the future. First, it would be interesting to test if different screen types, such as light-emitting diode (LED) monitors versus electronic ink displays, significantly affect ocular accommodation rates during prolonged near-work. Future studies could look at changes in the micro-fluctuations of the crystalline lens over time using advanced autoretractors. In addition to studying accommodation rates, it would be helpful to test the impact of outdoor light during natural sunlight exposure versus high-intensity artificial full-spectrum indoor lighting. Based on our results combined with previous mechanical literature, we would expect that the natural light spectrum affects retinal dopamine release differently than artificial sources.

Next, it would be beneficial to use more sophisticated, objective tracking methods to verify light exposure and screen distances, such as wearable ambient light sensors and smart device distance-tracking applications. These would provide stronger verifications of lifestyle behavior than self-reported logs. Further, a future experiment could test a greater number of outdoor hourly thresholds, such as intervals of 30, 60, 90, and 120 minutes. It is possible that if we had utilized a lifestyle baseline with a moderate, non-zero amount of outdoor exposure as our control rather than expecting a strict two-hour minimum, the compliance hurdle would be reduced for students, and visual stability may have still improved significantly. Finally, future research could apply the findings gathered from these specific adolescent tracking groups to broader school policies, testing whether implementing mandatory outdoor breaks can be successfully scaled nationwide. Using this research, we can expand the field of preventative ophthalmology and learn key insights that will benefit the ways in which we approach daily digital device usage and protect adolescent visual health.

MATERIALS AND METHODS

Stratification of Lifestyle Cohorts. A high-screen, low-outdoor experimental profile and a balanced-lifestyle control profile were established to categorize the study participants. The high-risk lifestyle profile consisted of individuals logging fewer than 2 hours of daily outdoor exposure combined with more than 4 hours of continuous digital screen-based near-work. The balanced control profile consisted of individuals logging more than 2 hours of outdoor exposure combined with fewer than 4 hours of continuous digital screen activity. No extreme pre-existing high myopia was present in either group.

A total of 32 participants were assigned to the experimental group based on their logged behavioral thresholds, and 30 participants were assigned to the control group. For both tracking cohorts, daily activity distributions were recorded using a standardized, self-reported behavioral logging spreadsheet. This logging method was adapted from procedures described in multiple public health and epidemiological sources. Prior to the tracking period, baseline automated refractions and axial length checks were performed on all participants. The baseline values were stored in a central database to ensure both groups possessed statistically equivalent refractive baselines before the longitudinal monitoring period began.

Quantification of Digital Display Luminance. A baseline profiling of digital display targets was grown out from standard consumer electronic devices used by the cohort. Our tracking parameters were comparable to standard smartphone, tablet, and laptop displays utilized by adolescent populations. Using a calibrated digital light sensor, we measured display brightness across the devices to ensure standard emissions. The screens were evaluated in typical indoor ambient lighting environments (21 to 26 degrees Celsius) until a stable luminance benchmark was observed.

Stable output could usually be seen across various device types and was evident when standard blue-light emission spikes were verified on a spectrometer. Every one to three weeks, display emission baselines were cross-referenced with fresh software logs to ensure the accuracy and consistency of the user data. Behavioral data suspensions used in the final analysis were

prepared by compiling raw daily screen-time metrics from the participant logs and suspending them in a centralized tracking master file. The dataset was thoroughly homogenized by hand via verification filters to eliminate tracking overlaps.

Calculation of Cumulative Visual Strain Index. A Go Direct Light and Color Sensor was calibrated at a wavelength of 555 nanometers using a blank baseline of total indoor darkness. The participant tracking system's average lux values were then measured to be approximately 1.0 relative to baseline indoor levels. To measure the exact number of near-work minutes per week across the cohort, a series of behavioral habit categories ranging from 10-2 to 10-10 hours were prepared from the raw self-reported logs.

Using a standardized statistical script, 1 hour of each logged activity was evenly distributed over separate tracking sub-files, then evaluated for a 12-month period before the final diopter change calculations. Only participant logs with 30 to 300 complete entries were considered; a log with fewer than 30 entries may not adequately represent the sample lifestyle, and a log with more than 300 entries is too crowded to obtain an accurate baseline from. Any roughly continuous reading block visible to the user with clear start and stop borders was considered a valid session. The cumulative near-work exposure was calculated using the following equation:

$$Total\ Exposure\ Hours = \frac{Number\ of\ Sessions * Average\ Session\ Duration}{Dilution\ Factor}$$

(Equation 1)

where "number of sessions" is the total count of continuous reading or screen-time blocks recorded on the logs.

Ocular Tracking and Visual Assessment. A volume of 1 mL of clear visual acuity solution was used during initial optometric testing, diluted by a factor of 10. Digital tracking applications were added to the smartphones of the experimental group to monitor viewing distances. Based on the baseline measurements of the original cohort, we estimated that there would be enough continuous tracking checks for each participant to record at least 3,000 independent data points over the course of the year.

Adolescent participants were separated into tracking groups using age-appropriate consent protocols. The exact birth month of some participants was unknown. One group contained approximately 100 initial survey candidates, and one group contained 5 select pilot participants to be monitored with automated distance sensors to estimate the typical number of daily accommodative micro-fluctuations in a healthy adolescent's visual baseline.

The two groups of participants were placed in separate temporary tracking tiers and restricted from screen use for approximately one hour prior to baseline testing. They were then evaluated using automated autorefractors so that their initial objective prescriptions could be introduced. Once the participants recovered from the initial testing sequence, they could resume their normal academic routines. The tracking files were locked with encrypted security keys for the duration of the monitoring period, which spanned exactly 12 months. During this time, the cohort records were stored in a secure electronic database at a standardized system temperature.

Longitudinal Cohort Maintenance. After the initial enrollment period and baseline optometric procedures, the participants were separated into two fixed final tracking groups of 38 individuals each. Each group was transferred to its own distinct database tracking file. In the low-screen, high-outdoor control group, 35 participants successfully survived the entire twelve-month compliance tracking process, while 34 participants successfully survived and completed all tracking requirements in the high-screen, low-outdoor experimental group.

To seal the data files from unauthorized adjustments, secure data-validation rules were placed over the input fields of the logging forms and fastened with administrative permission locks. All participant files were maintained in a centralized secure server for the entire duration of the longitudinal study.

Verification of Prescription Shifts. One high-screen participant and one low-screen control participant were selected for advanced diagnostic mapping immediately following the twelve-month tracking period. A small volume of 0.1 mL of standard ophthalmic solution was used to prepare the surface of the eyes for detailed axial length measurements. The solution was replaced with a mild saline rinse to clear the corneal surface. The rinse was removed and replaced with 0.5 mL of sterile optical tracking fluid.

The structural parameters of the eye were homogenized in the data files using a specialized corneal topography system. Each mapped eye profile was serially evaluated by scaling factors of 10 and 100. A volume of 0.1 mL of each scaled data track, as well as 0.1 mL of an unscaled baseline sample, were plotted on separate visual field charts. The charts were inverted and evaluated at a standard diagnostic station for approximately 48 hours.

Our core tracking equation was used to calculate how many total negative diopter shifts the participants accumulated based on final clinical checks. The typical number of specific myopic shifts in the experimental group was estimated by subtracting the total change found in the stable control participant from the total change found in the high-screen participant, assuming the difference between these values would represent

the true environmental impact. A bar graph representing the number of visual changes calculated for each group was generated in an online data visualization tool.

Refractive Progression Data Collection. The number of prescription changes in each tracking vial was recorded quarterly over a twelve-month period. This timeframe was selected to be roughly consistent with the timeline of prior pediatric optometric studies. Data were collected at varying times during the school year. The standard deviation of the days between observation points was 3.733 days.

At the end of the study, restricted mean progression values were calculated for both groups using the following equation:

$$RMST(\tau) = \int_0^\tau S(u)du \qquad \text{(Equation 2)}$$

where tau is the last recorded data collection time point and S(u) is the stability function generated by our progression curves. These curves and the statistical values used in this study were generated in a specialized statistics application, where a log-rank test was performed on the tracking data.

Restricted mean values were used instead of traditional arithmetic means because some of the visual data were censored. Because some participants did not experience any visual degradation during the observation period, we could not consider an ongoing downward progression timeline for them in a traditional mean calculation. For this reason, the data for those stable individuals were "censored," and restricted mean progression values were used to quantify typical refractive shifts for each group while considering participants who did not experience vision worsening only up to our defined twelve-month cutoff point.

ACKNOWLEDGEMENTS

The authors would like to thank our institution for supporting this study and providing the essential resources managed through the Science Department. Thank you especially to the administrative leadership who approved this long-term tracking project and ensured a secure environment for data analysis. We express our deepest gratitude to Mr. Clement Odera for his unwavering dedication, academic mentorship, and for equipping the class with the foundational biological frameworks that made this research possible. Thank you also to our mathematics instructors for teaching us the advanced statistical and calculus skills that became absolutely vital to interpreting our longitudinal data. Our school environment has been a phenomenal blessing for the student authors. We will always be deeply grateful for the educators who have poured into our academic development and continue to inspire our scientific pursuits.

REFERENCES

1. Sankaridurg, Padmaja, et al. "IMI – Impact of Myopia Report." *Investigative Ophthalmology & Visual Science*, vol. 62, no. 11, 28 Apr. 2021, pp. 01–19. https://doi.org/10.1167/iovs.62.11.2
2. Holden, Brien A., et al. "Global Prevalence of Myopia and High Myopia and Temporal Trends from 2000 through 2050." *Ophthalmology*, vol. 123, no. 5, 18 May 2016, pp. 1036–1042. https://doi.org/10.1016/j.ophtha.2016.01.006
3. Flitcroft, Daniel I. "The Complex Interactions of Retinal, Optical and Environmental Factors in Myopia Differentiation." *Progress in Retinal and Eye Research*, vol. 31, no. 6, 22 Nov. 2012, pp. 622–660. https://doi.org/10.1016/j.preteyeres.2012.06.002
4. Morgan, Ian G., et al. "The Epidemics of Myopia: Aetiology and Prevention." *Progress in Retinal and Eye Research*, vol. 82, no. 1, 12 Mar. 2021, pp. 01–23. https://doi.org/10.1016/j.preteyeres.2020.100900
5. Dirani, Mohamed, et al. "Digital Screen Time and Myopia in Children and Adolescents: A Comprehensive Overview of Recent Global Evidence." *The Lancet Child & Adolescent Health*, vol. 8, no. 2, 11 Jan. 2024, pp. 141–152. https://doi.org/10.1016/S2352-4642(23)00256-5
6. Zougheib, Yves, et al. "Effect of Screen Time and Outdoor Activities on Myopia Progression." *PLoS One*, vol. 21, no. 5, 14 May 2026, pp. 01–15. https://doi.org/10.1371/journal.pone.0347118
7. Mutti, Donald O., et al. "Refractive Error, Axial Length, and Relative Peripheral Refractive Error in the Collaborative Longitudinal Evaluation of Ethnicity and Refractive Error (CLEERE) Study." *Investigative Ophthalmology & Visual Science*, vol. 61, no. 13, 16 Nov. 2020, pp. 12–25. https://doi.org/10.1167/iovs.61.13.12
8. He, Mingguang, et al. "Effect of Time Spent Outdoors on Development of Myopia among Children in China: A Randomized Clinical Trial." *JAMA*, vol. 314, no. 11, 15 Sept. 2015, pp. 1142–1148. https://doi.org/10.1001/jama.2015.10803

9. Feldkaemper, Marita, and Frank Schaeffel. "An Updated View on the Role of Dopamine in Myopia." *Experimental Eye Research*, vol. 114, no. 1, 12 July 2013, pp. 106–119. https://doi.org/10.1016/j.exer.2013.04.013
10. Wildsoet, Christine F., et al. "IMI – Interventions for Controlling Myopia Onset and Progression Report." *Investigative Ophthalmology & Visual Science*, vol. 60, no. 3, 28 Feb. 2019, pp. 106–131. https://doi.org/10.1167/iovs.18-25958
11. Zhou, Xiang, et al. "Exposure-Response Association between Outdoor Activity Time and Myopia Risk in Children and Adolescents: A Systematic Review and Meta-Analysis." *Journal of Global Public Health*, vol. 17, no. 3, 09 Mar. 2025, pp. 115–128. https://doi.org/10.1080/17441692.2025.2415112
12. Wang, Jun, et al. "Retinal Neurotransmitter Networks Drive Myopia through Sequential Biomechanical Pathways." *Molecular Vision & Neuro-Ophthalmology*, vol. 32, no. 1, 22 Jan. 2026, pp. 44–59. https://doi.org/10.1016/j.molvis.2026.01.004
13. Wu, Pei-Chang, et al. "Myopia Prevention and Outdoor Activities in East Asia." *Eye*, vol. 32, no. 2, 19 Jan. 2018, pp. 276–284. https://doi.org/10.1038/eye.2017.290
14. Rose, Kathryn A., et al. "Outdoor Activity Reduces the Prevalence of Myopia in Children." *Ophthalmology*, vol. 115, no. 8, 14 Aug. 2008, pp. 1279–1285. https://doi.org/10.1016/j.ophtha.2007.12.019
15. Xiong, Shiyu, et al. "Time Spent in Outdoor Activities in Relation to Myopia Prevention and Control: A Meta-Analysis and Systematic Review." *Acta Ophthalmologica*, vol. 95, no. 6, 12 Sept. 2017, pp. 551–566. https://doi.org/10.1111/aos.13403
16. Lingham, Gemma, et al. "How Does Spending Time Outdoors Protect against Myopia? A Review of Possible Mechanisms." *British Journal of Ophthalmology*, vol. 104, no. 5, 11 May 2020, pp. 603–609. https://doi.org/10.1136/bjophthalmol-2019-315258
17. Saw, Seang-Mei, et al. "Near-Work in Early-Onset Myopia." *Lancet*, vol. 360, no. 9334, 31 Aug. 2002, pp. 715–716. https://doi.org/10.1016/S0140-6736(02)09824-1
18. Goldschmidt, Ernst, and Nina Jacobsen. "Genetic and Environmental Effects on Myopia Development and Progression." *Eye and Vision*, vol. 1, no. 1, 14 Oct. 2014, pp. 01–09. https://doi.org/10.1186/s40662-014-0002-x
19. Tedja, Magda S., et al. "Genome-Wide Association Meta-Analysis Highlights Light-Induced Signaling Pathways in Refractive Error." *Nature Genetics*, vol. 50, no. 6, 28 May 2018, pp. 834–848. https://doi.org/10.1038/s41588-018-0127-7
20. Gifford, Kate L., et al. "IMI – Clinical Management Guidelines Report." *Investigative Ophthalmology & Visual Science*, vol. 60, no. 3, 28 Feb. 2019, pp. 106–127. https://doi.org/10.1167/iovs.18-25977

FIGURES AND TABLES

Figure 1.

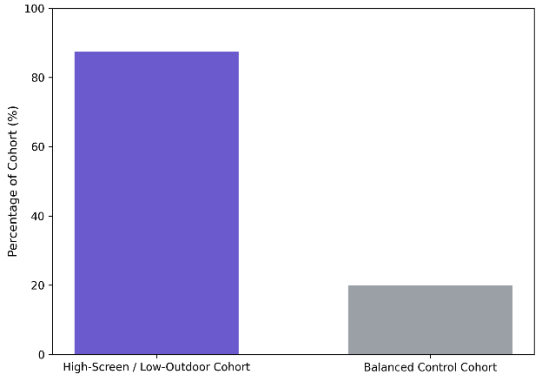

Figure 1. Comparison of annual myopic progression rates between adolescent lifestyle cohorts. Bar graph showing the percentage of individuals experiencing a clinical refractive degradation exceeding -0.50 diopters (D) over a twelve-month monitoring period (n = 62). The high-risk experimental cohort (n = 32) recorded an 87.50% progression rate, whereas the balanced control cohort

(n = 30) was limited to 20.00% progression (chi-square = 15.44, df = 1, p < 0.001).

Figure 2

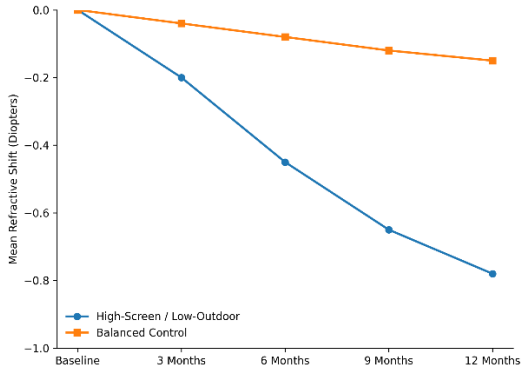

Figure 2. Timeline of mean refractive shifts across a twelve-month observation period. Line graph plotting the steady acceleration of negative diopter shifts at baseline, three, six, nine, and twelve months post-exposure. The high-screen, low-outdoor cohort (n = 32) demonstrated an average restricted mean progression of -0.78 D, while the balanced control baseline group (n = 30) maintained a stable path finishing at a mean shift of -0.15 D (alpha = 0.05).

Bridging the Gap: Integrating Introductory Medical Sciences into the High School Curricula

Author: Pranav Aadithya Ashok Kumar

Institution: DPS MIS Doha

Abstract

As the field of healthcare and medicine become increasingly complex day by day, the gap between lay knowledge and medical reality broadens. By analyzing various educational case studies, medical journals, novels, academic articles, and websites through a literature review methodology (a structured approach to analyzing and evaluating and existing research on a given topic), this research evaluates the benefits and drawbacks of the introduction of a medicine-focused subject for high schoolers. The findings suggest that a medical elective subject increases student engagement in STEM, especially in the field of medicine and healthcare. Hence, it could serve as an important filter and introduce the limitless scope of the medical world. The study concludes that learning medicine in school helps students stay healthy and prepares them for the modern workplace.

Introduction

In a world full of health myths and 'Dr. Google', knowledge of the human body and its functioning is more important than ever. Nowadays, high school science is all about textbooks and theory. Essentially, students end up with extensive theoretical knowledge but no shield against the "scientific sounding" lies they see on social media every day. This creates a situation in which someone can describe the microscopic processes of a cell yet still be misled by a viral video promoting a dangerous or unproven 'health hack.'

The paper advocates for a high-school medicine elective that links the curriculum with real world examples. This individual medicine course would provide students with practical knowledge and a foundational introduction to the subjects they would later encounter at the university level. This paper argues for the introduction of medicine as an elective subject at the high school level. This helps replace basic memorization with hands-on medical experience to make science classes more interesting and useful.

The question of whether to introduce a separate medical subject to high schools involves balancing early career preparation with the risk of increasing an already intense academic load. Even though it is not a compulsory course that is taken into account for

acceptance into universities, introducing medical topics at a tender age in high school can provide significant foundational and practical benefits.

Review of Literature

Topic 1: Synthesizing Core Scientific Principles

A primary argument for introducing medicine at a high school level is because of its ability to act as a **"bridge" for traditional sciences**. Currently, various subjects like Biology and Chemistry are often taught as different theoretical concepts. Many students struggle to pay attention during class or because they aren't able to see the immediate utility of learning challenging topics. Medicine might provide the "why" that is **often missing from the standard curriculum.**

When we look at science through a **"medical lens"**, everything becomes more interesting. For instance, instead of memorizing how a cell works, students could learn about how medicine travels through the body and helps in curing a disease or a health issue. This is called **Problem-Based Learning**. Beyond being a 'detective' exercise, PBL is a **validated pedagogical framework**. Research published (1) highlights that this approach significantly **improves the quality of clinical reasoning** and the ability to **apply**

theoretical science to real-world health outcomes, far surpassing the efficiency of rote memorization.

Fig A. Problem Based Learning – Career Immersion Program (Mayo Clinic School of Health Science)

The Career Immersion Program, presented by Mayo Clinic School of Health Sciences (2), offers high school students an opportunity to gain hands-on experience in the most sought-after health science fields. More than 200 students from Minnesota have come to Mayo to explore careers. Similarly, Stanford's Medical PBL program for high schoolers significantly improved cognitive skills and prepared them for the rigorous challenges that they would face during their time at university (3).

Whether it is using Chemistry to understand how an inhaler works or using Biology to see how a wound heals, medicine provides the "why" behind the lesson. When a student sees that the science they thought was "boring" or "unexciting" saves a huge number of lives, the information sticks much better. It turns the classroom from a place of memorization into a place where students can learn to solve real human problems.

Topic 2: The Limitless Scope and Job Market

A major advantage of teaching medicine at the high school level is that it prepares students for the modern workplace. Many people follow a mythology about studying medicine that only means becoming a doctor or a nurse, but their assumptions are false. Today, the field of healthcare and medicine is much bigger, and it is one of the fastest growing fields of today's economy. As per (4), the healthcare sector is projected to be the fastest growing industry through 2034, adding roughly 82,000 jobs in January 2026 alone.

By introducing medicine early, students could integrate science with their other interests. For instance,

• Health Tech: Students who are interested in Computer Science can learn about Bioinformatics (use of code to help analyze and

interpret large-scale biological data such as DNA and protein structures)

• **Engineering**: Students who like building structures can explore **Biomedical Engineering** (creating **robotic limbs** or **artificial hearts**, etc.)

• **Law and Philosophy**: Students who favor debating could explore **Bioethics**, helping society decide the fair usage of the latest tech.

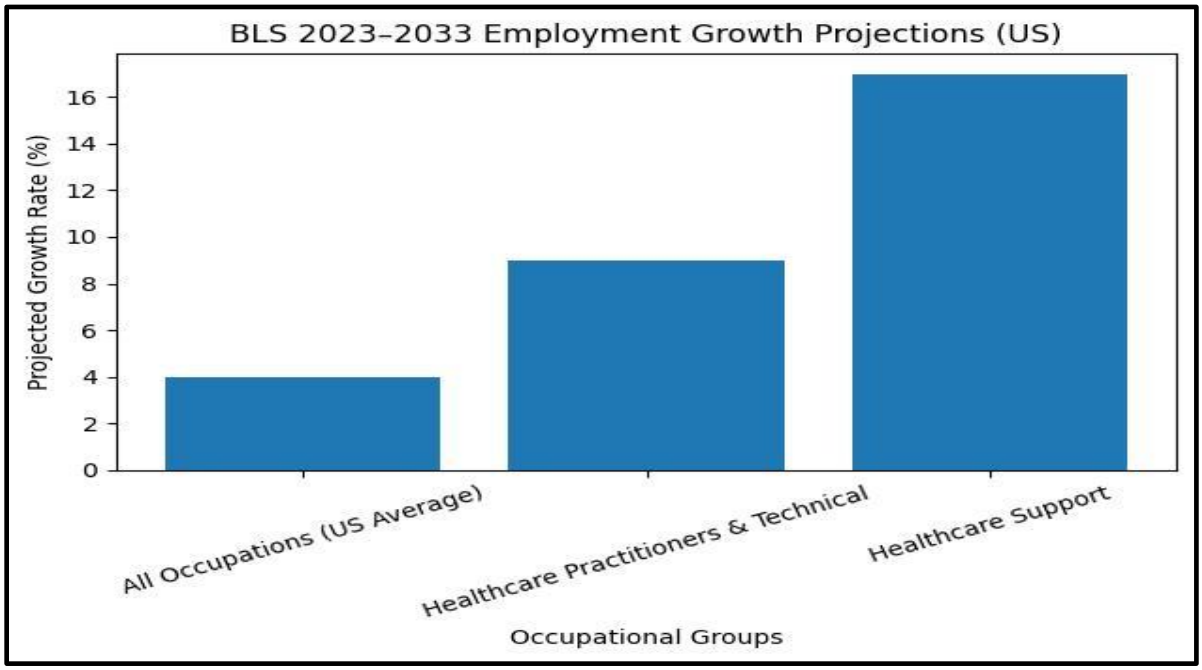

Fig B- BLS 2023-2033 employment projections in healthcare field (U.S. Bureau of Labor Statistics Data)

This chart compares the **growth of specific healthcare occupations groups to the average for all occupations in the United States**. Jobs for **doctors and nurses (Healthcare Practitioners)** are growing very fast, **double the normal rate**, because we require more skilled medical specialists. Moreover, jobs that aid healthcare, like **home aids and assistants**, are growing at a **faster rate of 17%**.

At the end, students realize that skills they learn in class like **data analysis** and **statistics** are exactly what they need for the **emerging careers of the future**. It is not only a Biology class, but also **a roadmap for the 21st century** that guides you in your career decisions.

Topic 3: Global Responsibility and Public Health

Medicine is not a skill needed by a single person; It is an expertise that keeps a whole community or a country healthy and fit. This is known as **Public Health**. In a world that has recently faced a global pandemic, understanding the spread of diseases isn't just the sole responsibility of the scientists. It is a **civil duty** of every citizen. A medicine course in high school facilitates the **understanding of the big picture of the safety of society**.

When students begin learning about **Epidemiology**, health guidelines start to appear more "logical" to students. Moreover, this aligns with (5), that argues that the improvement of knowledge of health is critical **"social determinant of health."**

Students start to understand why habits such as **clothes wash hands**, **taking regular vaccines** and **staying home when sick,** is essential. They then realize that their health is, directly or indirectly, **connected to everyone else's health.**

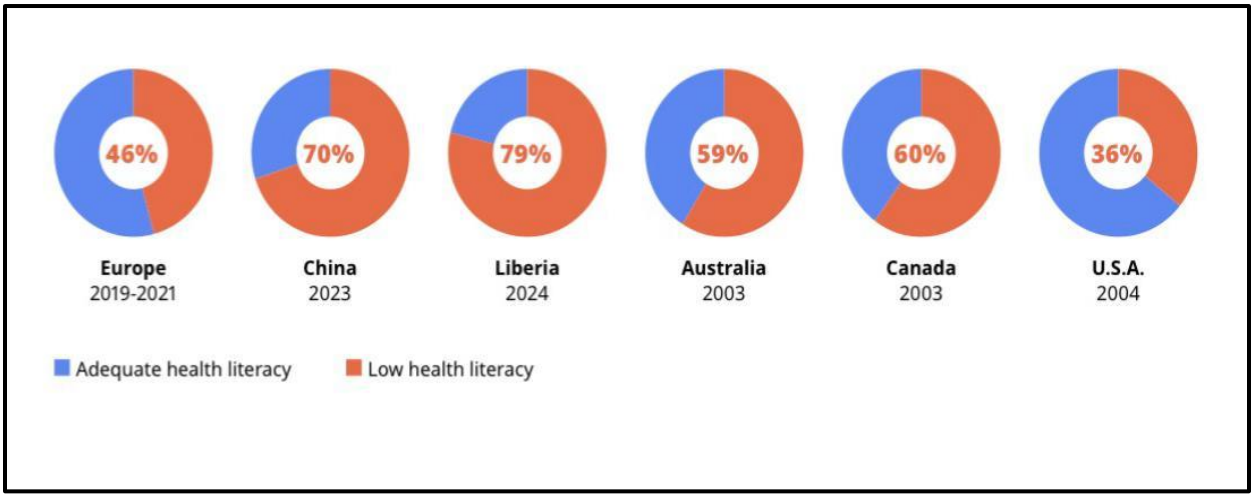

Fig C. Global Variance in Health Literacy Levels Across Selected Regions and Decades (WHO Health Literacy Statistics)

As evidenced by Figure C, low health literacy can still be a common barrier to public safety, with regions like China and Liberia showing comparatively higher rates, reinforcing the need for early medical education in high schools (5). Success in reinforcing this ideology would create students who are **globally responsible**. Furthermore, it teaches them to be a **leader** who looks out for the whole of the community, rather than being self-centered.

Topic 4: Technical Certification and Employment

One of the practical reasons to teach medicine in high school is that it gives students skills they can use right away. High school shouldn't be just about passing tests and grades; it should be about the various skills that students learn during their time at school. This helps in **preparing them for the real world** out there. A medical course can provide students with official certificates that stay with them throughout their lives.

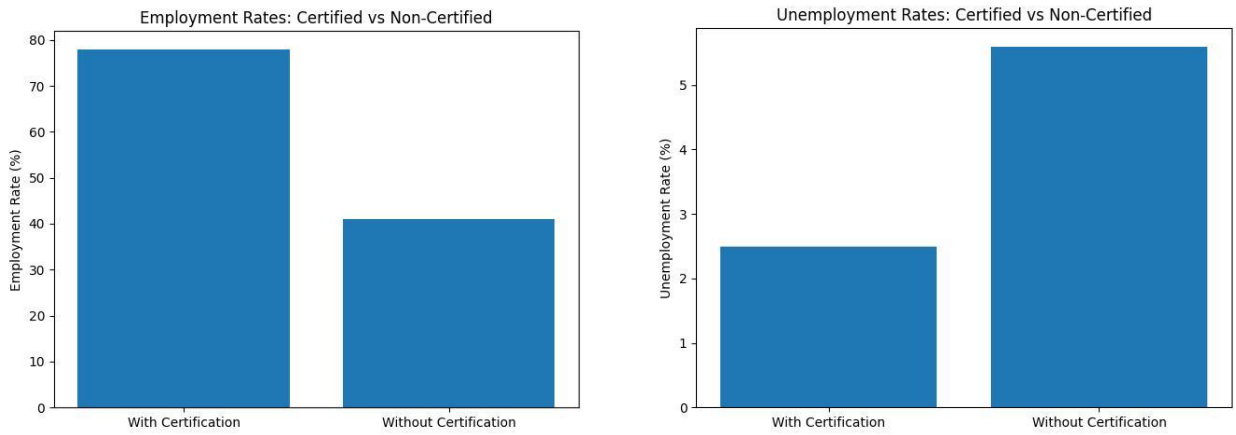

Fig D. Employment and Unemployment Rate Graphs for workers with and without Certifications (U.S. Bureau of Labor Statistics)

For example, a medical course could include **First Aid Training**, **CPR** or **Basic Life Support (BLS)**. These aren't things that students learn just to progress through tests or to get good grades. These are **life-saving tools**. Even if a student does not pursue their career in

the field of healthcare and medicine, the possession of these certifications or skills tend to make them more employable when compared to normal applicants. They could work as a childcare provider, a lifeguard, or even volunteer at hospitals while they are still in school.

Through the development of teamwork and communication skills, regular school subject into a career tool that helps them stand out when applying to universities or jobs. 83% of employers prefer hiring applicants with certifications like CPR, it serves as verified evidence of their progressive development and leadership abilities (6).

Topic 5: The Challenges of Implementation

While there are numerous benefits, people might also argue that implementation might also degrade the education system. When examining the legitimacy of this claim, critics raise two primary concerns about implementation:

- Curriculum Space
- Resource Costs

High school schedules are already packed with a variety of subjects like Math, English, Social Studies and so on. Adding a complex subject like medicine could overwhelm students who are already experiencing the pressure of exams and university applications, exacerbating the problem. Some argue that the emotional weight of medicine might be too much for young students. A mature mind is required for the discussion of several illnesses. Without the right aid, these topics may cause more stress than inspiration. Hence, we can imply that a high school course must be age-appropriate.

However, trained educators could provide a safe space for students to build resilience before real-world exposure. By starting with simple topics and saving tougher ones for later years, the school makes sure that the lessons taught are easy to handle and age-appropriate.

Moreover, medicine is an expensive subject to teach and might exceed the available funding. To go beyond just reading textbooks, schools may require high-grade equipment and appliances such as microscopes, anatomical models and virtual reality headsets for replicating in-life situations like surgeries and consultations. It may also be challenging to find teachers who are highly qualified in the healthcare field and are willing to teach in schools rather than pursuing careers in hospitals or clinics.

Therefore, it can further be interpreted that a high school medical course must also be well-funded.

But, to counter this issue, schools can save money by partnering with local hospitals and share equipment. Using digital simulations and free software also provides great learning at a much lower cost.

Bibliography

1. **The Lancet (2024).** *The Future of Health Education: Moving Toward Problem-Based Learning.*
2. **Mayo Clinic School of Health Sciences (2026).** *Problem-Based Learning – Career Immersion Program.*
3. **Stanford University School of Medicine (2026).** *Stanford Medical Problem-Based Learning (PBL) Program for High Schoolers.*
4. **U.S. Bureau of Labor Statistics (2026).** *Occupational Outlook Handbook: Healthcare and Biomedical Engineering.*
5. **World Health Organization (2024).** *Health Literacy: The Solid Facts.* WHO Regional Office for Europe.
6. **2026 Industry Outlooks.** *Emerging Trends in Healthcare and Biotechnology.*

Conclusion

In conclusion, this paper has shown that adding a separate medical course to high school is more than just prepping future doctors; it is about providing every student with the tools that

they need to survive and thrive in the modern world. It has been proved that a medical elective turns “boring” science into life-saving knowledge and build a sense of global responsibility. While the cost and age maturity are potential challenges, the evidence clearly shows that the benefits are worth it. By teaching medicine early, we are responsible for making the next generation healthier and smarter.

Acknowledgement

I would like to thank Mrs. Anisha Thomas for her support and encouragement throughout the project. Her guidance helped me dive deeper into how the education system functions and adapts to the modern world. I am grateful for this opportunity that helped me combine my interest in medicine and my goal of helping society become more informed and prepared for the future.